Cranfield

College of Aeronautics Report 8408
March 1984

The Subsonic Aerodynamic Characteristics of a Body of Revolution – A Revised Experiment.

by P.A.T. Christopher, Z. Hussain and C.T. Shaw

College of Aeronautics
Cranfield Institute of Technology
Cranfield, Bedford, U.K.

Cranfield

College of Aeronautics Report 8408
March 1984

The Subsonic Aerodynamic Characteristics of a Body of Revolution – A Revised Experiment.

by P.A.T. Christopher, Z. Hussain
and C.T. Shaw

College of Aeronautics
Cranfield Institute of Technology
Cranfield, Bedford, U.K.

ISBN 0 947767 00 2

£7.50

SUMMARY

This report, which is a natural sequel to Ref.3, presents the results obtained from a series of wind tunnel tests on an axi-symmetric body. These tests were conducted in a subsonic tunnel at a nominal Reynolds number of 580000 and measured the distribution of pressure on the body when set at a range of incidences from -2 degrees to +5 degrees. Using the measured pressure coefficients, load distribution, normal force, pitching moment and centre of pressure results were obtained.

Comparison and correction of the measured data was obtained through the use of the panel method SPARV. The opportunity was taken to compare the RING SOURCE method, which was designed to deal with the potential flow around bodies of revolution, with inviscid SPARV.

CONTENTS

Section		Page
1.0	INTRODUCTION	1
2.0	EXPERIMENTAL ARRANGEMENT	2
	2.1 The model	
	2.2 The support rig	
	2.3 Instrumentation	
	2.4 Test procedure	
3.0	THEORETICAL PREDICTIONS	5
	3.1 The panel method (SPARV)	
	3.2 The RING SOURCE method	
4.0	EXPERIMENTAL RESULTS	7
	4.1 Distribution of normal loading	
	4.2 Pressure distribution	
	4.3 Normal force coefficient	
	4.4 Pitching moment coefficient	
	4.5 Centre of pressure location	
	4.6 Correction to incidence	
5.0	DISCUSSION OF INTERFERENCE EFFECTS	14
	5.1 The old rig	
	5.2 The new rig	
	5.3 Possible sources of interference	
	5.4 Comparison between old and new rigs	
6.0	COMPARISON BETWEEN THE THEORETICAL METHODS	18
7.0	IMPLICATIONS FOR FURTHER TESTS	19
8.0	CONCLUSIONS	20
	REFERENCES	21
	APPENDICES	

1.0 INTRODUCTION

As part of a programme of research into the aerodynamic interference between axi-symmetric stores, an experiment was conducted on the basic store, Ref.3, in which it was found that the results were, due to interference from the support rig, unsatisfactory. This rig has now been re-designed and manufactured and the present report gives an account of the new series of tests and the comparison of experimental results with theoretical predictions. Implications for planned multi-body experiments are included.

2.0 EXPERIMENTAL ARRANGEMENT

2.1 The Model

Since the theoretical predictions which were to be used would not include separated flow a body was required which would have attached flow along the greater length of the body but still have significant viscous effects at low incidence. An ogival nose with a three-degree-slope boattail was chosen as the body shape. The boattail and the long length of the body, about 1.53 metres, should allow a relatively thick boundary layer to develop over the rear of the body whilst remaining attached. A trip wire was placed near the nose of the body to force the boundary layer to become turbulent.

The basic model comprised four aluminium sections, joined together, and supported by bearings onto a rigid steel shaft. A stepper motor giving 400 steps per revolution was located in the nose to allow rotation and was fixed by a universal joint to the steel shaft. Along one meridian plane 36 pressure tappings were located and fed by flexible plastic tubing to a 48-port scanivalve containing a 0.1 psid pressure transducer. Also, two sets of four holes (at 90 degrees intervals) were located at two positions along the length of the body. A sketch of the model used in the tests is shown in Fig.1 and the positions of the stepper motor and scanivalve are shown by Fig.2.

2.2 The Support Rig

A schematic diagram of the initial support rig is shown by Fig.3 and clearly shows the side fairings and back strut. The redesigned rig is shown in Fig.4. It comprises a sting into which the model was located. The other side

of the sting was located into a bracket fixed to the middle of a rectangular cross-section, hollow strut which spanned the tunnel height. The new rig uses a tail wire arrangement similar to that used previously. The back strut was unfaired.

2.3 Instrumentation

A Pitot-static tube was used to measure the free stream total head. The measurement was made at a distance of 0.3 metres from the tunnel wall by a 0.5 psid pressure transducer. The static pressure from the Pitot-static tube was also connected to a T-junction inside the model. One joint of the T-junction was connected to the transducer and used as the reference pressure, with the other joint connected to port 1 to give a zero error reading for the transducer. An analogue to digital converter was used to convert the signal from both transducers suitable for input into a Commodore PET computer. This computer also controlled the stepping of the motor, using a drive/interface combination, and the scanivalve. Fig.5 shows the instrumentation used in the tests.

2.4 Test Procedure

The tunnel was calibrated for six incidence cases, namely, 5,4,3,2,0,-2 degrees. The tunnel speed was calculated to give a nominal Reynolds number (based on model maximum diameter) of 580000 and the model was set at its initial roll angle. All 48 ports were scanned in sequence, port 1 being connected to the free stream static pressure to give a reference zero error. The free stream total head was measured every time a port was scanned. Due to the relative sizes of the model and support rig cross-sectional area as compared with the tunnel working section cross-sectional area the readings were not corrected for blockage

effects. The measurements were recorded onto a disc in sets of 48, at 11 roll settings. Calculation of the loads and pressure distributions was carried out later by a separate programme.

3.0 THEORETICAL PREDICTIONS

3.1 The Panel Method (SPARV)

The panel method essentially approximates the body surface. In two-dimensional flow the body contour is split up into connecting lines. In three-dimensional flow the body surface is approximated by facets. By using a large number of panels the approximated body surface resembles the original quite well resulting in a highly accurate answer which is close to a possible exact solution. Usually the number of panels used is dependent on the complexity of the body shape and user experience. With a body such as the present one, which does not have a pointed base, a wake enclosure has to be specified. The type of enclosure chosen is largely arbitrary but usually resembles the shape of the body nose region. See Ref.2.

The model, sting and back strut were represented as three components. The body was modelled by 15 axial panels and 15 circumferential panels. The sting was modelled by 13 axial panels and 15 circumferential panels. Due to the dimensions of the back strut, length to width ratio of about 2, the flow would be expected to separate near the nose and reattach along the aft of the strut. This could be regarded as an oblate ellipse and was modelled as such, with 19 axial panels and 15 circumferential panels. The wake enclosure used was a linear one extending to the surface of the sting.

3.2 The RING SOURCE Method

The RING SOURCE method (Ref.4), was designed for bodies of revolution alone and is useful for quick comparisons with experiment. The body is divided into frusta, with the nose and tail region frusta being cones. The sources

form rings on the frusta and each ring has a constant source strength distribution. The number of control points is dependant on how many frusta the body is divided into, unlike SPARV, where the number of control points is dependant on the number of axial and circumferential panels. With SPARV the size of the matrix set up is far higher than that with the RING SOURCE method.

The theory is linear and, therefore, flow at incidence can be divided into an axial component and a crosswise component. With the crosswise component the source strength varies as a SINE or COSINE function of the meridian angle.

The result of the RING SOURCE method is a fast and accurate method, with a smoother surface than SPARV, for calculating the potential flow around bodies of revolution.

4.0 EXPERIMENTAL RESULTS

4.1 Distribution of Normal Loading

The raw data stored on the disc comprised the x location of each port, the reading from the transducer in the model, the pressure coefficient, the total head reading and the roll angle. By a numerical integration technique the value for the normal loading at each port could be found. In this series of tests the trapezium rule was used as the integration technique. Figs.6 to 11 show the experimental results compared with the theoretical predictions. The theoretical method used was that of Ref.1.

The panel method programme (Ref.1) was run at the incidence cases that the body was tested. However, it was found that the peak load of the experiment did not agree with that obtained by the panel method. As the flow is attached over the nose region of the body, and can be regarded as being inviscid, the peak load should be predicted accurately. Fig.12 was drawn from the inviscid SPARV (Ref.1) runs and from this the peak load was found and plotted against the angle of incidence, Fig.13. From this the true angle of incidence was found.

Overall the general comparison between experiment and theory was good and the serious interference experienced with the previous rig was not present, but several points of interest arose:

(a) At an incidence of 5 degrees the position of peak load in the experiment agrees with that obtained with SPARV. However, at lower incidences the agreement is not so good. The peak load in the experiment is behind that obtained from the theoretical predictions at positive incidences and forward at negative incidences. The degree

of mismatch gets worse as the incidence approaches zero. This is in accordance with the findings of Christopher and Shaw (Ref.3).

The theoretical predictions do not include any variation of incidence along the length of the body. It had been found that there was a variation of incidence of the flow in the wind tunnel across the height of the tunnel (Sec.4.1), so at each port location along the body length the effective angle of incidence changes. This characteristic cannot be modelled by the SPARV panel method and, therefore, must be considered when comparing the theoretical predictions with the experimental results.

(b) At positive incidences the minimum down load is well predicted and maintained towards the base. However, at an incidence of 5 degrees the flow has possibly separated near the base and the loading increases but does not reach zero at the base. At lower incidences the load near the base region has a tendency to decrease. The effect is more pronounced at the negative incidence cases where the loading decreases from a positive value near the beginning of the boattail to a negative value near the base. However, the trend is in one direction. There is obviously interference from a source near the base at these lower incidence cases. Possible sources of the interference are discussed later.

(c) The viscous SPARV solution (involving a transpiration velocity concept) is that obtained after one iteration. The theoretical load increases along the boattail at positive incidences and decreases along the boattail at negative incidences. This trend is in accordance with the experimental results, but the agreement between the theoretical and experimental results along the boattail is not good, even with a higher number of viscous

iterations (Fig.14). The viscous SPARV results show that at 4.85 degrees incidence the flow separates near the base, showing the disagreement with the experimental results. This separation is due to large normal velocity components which can be suppressed in SPARV, but have not been done so here.

To test whether the disagreement along the boattail would be decreased by conducting further viscous iterations, SPARV was run with eight viscous iterations at 2.65 degrees incidence. The result is shown by Fig.14. The difference between the results for the third and subsequent iterations is very small and so, the results for the fourth and higher iterations have been excluded from Fig.14. However, there is still poor agreement with the experimental results.

4.2 Pressure Distribution

The variation of pressure coefficient with distance along the body from the nose is shown by Figs.15 to 20. In all the cases it can be seen that over the nose region the theoretical values agree well with the predicted values. The pressure 'bucket' is well predicted at all the incidence cases. There is a divergence from the experimental values towards the aft region of the body, near the base. Furthermore, at the negative incidence cases the value of C_p for the zero roll angle is less than that for the 180 degrees case. The curves 'cross over' at X/L = 0.30 and then again at X/L = 0.71 for the zero incidence case and X/L = 0.68 at the 2 degrees case. This, once again, shows the presence of interference near the base region. This could be attributed to the asymmetry of the boundary layer along the body which gets progressively worse towards the base and for reasons which will be discussed later in Sec.5.3.

The experimental pressure coefficients are given in tabular form in Appendix B.

4.3 Normal Force Coefficient

The normal force coefficient variation with angle of incidence, corrected and uncorrected, is shown by Fig.21. To find the correction to incidence a straight line was drawn through the origin and the value of the load at 4 degrees incidence. This was because the correction to the incidence at 4 degrees was very small and also, because at zero incidence the load should be zero. Over this range it was assumed that the normal force coefficient versus incidence curve was linear. The value at an incidence of 1.50 degrees does not lie on the line. The pressure was investigated and it was found that the discrepancy arose due to effects near the base region. The value at -2.85 degrees incidence is well off the line and is possibly due to the interference from the sources that will be discussed later. At 4.85 degrees incidence the flow towards the base is viscous dominated and may be very near to separating. This would account for the curvature of the C_n versus incidence line above 4 degrees incidence. At a positive incidence the normal force coefficient is of the same magnitude but of opposite sign at the corresponding negative incidence.

Usually, force and moment measurements are made in the wind tunnel. If the normal force versus incidence curve does not pass through zero, it is normal practice to 'shift' the whole curve so that it does. So, in effect, a zero incidence shift is applied at all incidences to the uncorrected readings. This is shown in Fig.21. The slope of this curve is greater than that for the corrected incidence case.

4.4 Pitching Moment Coefficient

The model could be regarded as a very sensitive yaw meter, the sensitivity of which is shown by Fig.22. Looking first at the pitching moment versus incidence curve, for pitching moment measured about the nose, the values at the negative incidences are not in good agreement with the rest if a straight line is expected to fit the points. The value at -2.85 degrees incidence is nearly zero. The pitching moment is very dependent on the flow characteristics near the base due to the long moment arm (moments were measured from the nose). By considering the load versus incidence curve at -2.85 degrees, Fig.11, it can be seen that the departure can be attributed to the nature of the flow near the base. However, if the moments are taken about the base the values obtained for C_m give a linear variation of pitching moment with incidence (Fig.22). A straight line passing through zero is obtained and the correction to incidence is in agreement with that obtained using peak loads. (Fig.13).

Once again, adopting the usual practice of applying a zero incidence shift to all incidences, a curve passing through zero was obtained. This curve, Fig.22, as with that for the normal force coefficient, is symmetric and of greater slope than the corrected incidence case.

4.5 Centre of Pressure Location

By dividing the pitching moment by the normal force coefficient, X_{cp}, the location of centre of pressure, is obtained in calibres (model maximum diameter). Table A in Appendix A, shows the variation of X_{cp} with incidence. It can be seen that at an incidence of -2.85 degrees the centre of pressure is located at the body nose. At all the other incidence cases the location of the centre of

pressure is forward of the body nose and is furthest forward at an incidence of 2.65 degrees.

Using the method of Brebner (Ref.5), which is semi-empirical, the location of centre of pressure has been obtained, for the present body, at all incidences. The results are shown in Table A. It can be seen that the agreement with the experimental results is good at 1.50 and 3.95 degrees incidence, but is poor at the other incidences.

The usual method of predicting the centre of pressure position is by dividing the gradient of the pitching moment coefficient curve by the gradient of the normal force coefficient curve. This results in one value for X_{cp}, which in this series of tests is 0.870 calibres ahead of the nose for the corrected incidence case and 1.847 calibres for the uncorrected incidence case. The value of X_{cp}, for the zero incidence shift case was found to be the same as the uncorrected incidence case and was located at 1.847 calibres ahead of the nose.

4.6 Correction to Incidence

Three methods have been used to find the correction to incidence:

(a) Peak loads from the theoretical predictions (Fig.13).

(b) Normal force coefficient (Fig.21).

(c) Pitching moment coefficient (Fig.22).

The peak loads (Fig.13) give the correction to incidence according to inviscid flow. However, since the flow over the nose region is essentially inviscid, the corrections

obtained can be accepted as being true. The correction for the zero incidence case, by this method, is -0.85 degrees.

The normal force coefficient curve for the uncorrected case passes through 0.75 degrees for zero load, resulting in a correction to the incidence of -0.75 degrees at zero load for the curve to pass through the origin.

The pitching moment coefficient curve passes through 0.70 degrees for zero pitching moment resulting in a correction to incidence at this case of -0.70 degrees, for the curve to give zero moment at zero incidence.

The disagreement between the three methods is very small and arises due to the normal force being obtained by integrating the normal force at each port location over the whole body, resulting in an accumulation of any error in the incidence along the body. Similarly, the pitching moment coefficient has a larger error due to the moment arm. However, the consistency between the answers is very good.

5.0 DISCUSSION OF INTERFERENCE EFFECTS

5.1 The Old Rig

The interference effects of the old support system (Ref.3) were quite evident from the findings of the authors. The main areas of interference arose from the side fairings and the circular back strut. The reasons for which are explained in, Sec.5.4.

5.2 The New Rig

Fig.4, shows the new rig and the model. The back strut is located at 0.76 metres behind the base of the model. By conducting theoretical investigations using inviscid SPARV (Ref.1) it was found that the presence of the back strut had little effect on the flow over the model. It was also found that the effect of the sting was minimal, only affecting the pressure coefficient near the base in the third decimal place of significant figures. Further, earlier SPARV runs showed the absence of any effect from the tunnel walls. There remains only the wire from the base of the model, the jubilee clips and the wires and pressure tubing leading down through the tunnel floor (Fig.4) as possible sources of interference. The wire from the base of the model protrudes into the flow, due to the need for the model to roll. Three of the jubilee clips could effectively lie in the wake of the body but the most rearward clip could contribute to the interference experienced near the base. Also, the wiring and tube leading down through the tunnel wall could also contribute to the interference.

5.3 Possible Sources of Interference

It is evident from the loading curves that the interference arises at the lower incidences. However, it may also be

present at the higher incidence cases but could be dominated by viscous effects near the base.

In Sec.5.2 the possible sources of interference were discussed and we now proceed to elaborate on the effects of each on the flow near the base of the model.

(a) The wiring and tube leading away from the model down through the tunnel floor could be regarded as a circular cylinder and contribute to the interference. The effect would be to slow the flow down near the base of the model.

At positive incidence the flow on the top surface is travelling slower than that on the bottom surface of the model. The effect of the circular cylinder would be to slow the flow down even further on the top surface. This would result in an increase in pressure on the top surface leading to an increase in download near the base and an overall decrease in normal force.

At negative incidence the flow on the top surface travels faster than that on the bottom surface. In this case the circular cylinder would slow the flow down on the top surface, which leads to a decrease in upload near the base and an overall increase in the download.

These effects are in accordance with the findings from the experimental results.

(b) As the three clips closest to the model base may effectively lie in the body wake only the most rearward clip will be considered.

At positive incidence the clips are on the meridian plane corresponding to a roll angle of 180 degrees, i.e. the

bottom surface. The most rearward clip may not allow the wake flow to re-attach to the sting resulting in an effective thickening of the wake towards the bottom surface. The consequence is that the flow travels faster and the pressure decreases on the bottom surface leading to an increase in download near the base.

Further, at negative incidence the wake thickens on the bottom surface resulting in the flow travelling faster than it would without the clip being present. The upload near the base, therefore, decreases.

This, once again, is in accordance with the experimental results.

(c) The base wire protrudes, by its greatest amount into the flow at a roll angle of zero and at 180 degrees roll angle the wire is taut and lies in the body wake. The effect of the base wire would be to separate the flow on the bottom surface near the base leading to a decrease in download at positive incidence and an increase in upload at negative incidence.

This is not in accordance with the experimental results.

5.4 Comparison Between Old and New Rigs

By comparing the loading curves obtained in the initial experiments (Ref.3) to those obtained in the present experiments it can be seen that the interference due to the support rig has been considerably reduced. The side fairings and circular back strut have been replaced by a slender sting and rectangular cross-section back strut.

The previous rig affected the flow over the whole body. The side supports, which were faired with aerofoil type

tapered sections, caused a speed-up in the flow at the mid section of the body. There was also asymmetry of the flow due to the side supports extending down only half of the tunnel height. Therefore, at negative incidences (measured upwards) the body was between the supports and at positive incidences the body was below the supports. The flow may also have been affected by the three-dimensional effects at the support ends. Further, the circular back strut slowed the flow down near the base by pushing it outwards and around itself.

The new rig, however, does not suffer from these drawbacks. The back strut is far enough behind the base of the model to have little effect on the flow in the base region.

6.0 COMPARISON BETWEEN THE THEORETICAL METHODS

SPARV has the capability of dealing with multi-component flows, and can deal with a complete aircraft configuration, the limit being set by the computer size and the cost. Therefore, it can deal with complicated flows, such as that with axi-symmetric bodies in close proximity to each other, to name but one. There is also a capability for viscous flows.

Wind tunnel interference corrections can now be estimated comprehensively with SPARV, as compared to the traditional estimates, which were confined to blockage and incidence.

The RING SOURCE method has, so far, been confined to inviscid flows about isolated bodies of revolution (Ref.4). The main advantages of the method are that the input to the developed computer programme is far easier and shorter than that for SPARV, and, most important of all, the run times are shorter.

Figs.23 to 28 show the inviscid SPARV results, for the boattail store used in the experiment, compared with the RING SOURCE method. It can be seen that the agreement is very good over the whole incidence range.

7.0 IMPLICATIONS FOR FURTHER TESTS

It has been shown that with the new rig the interference has been reduced significantly relative to the old rig (Ref.3). However, at lower incidence some interference is still present, but it is hoped to eliminate this by keeping the 'back wire' from protruding into the flow by keeping it taut, possibly by a spring system, and to exclude having to use some or all of the jubilee clips.

The new rig has been shown to be a sound support system on which to conduct single body tests, and it is hoped it will be suitable for conducting planned multi-body tests, where the range of roll angle will have to be increased to 360 degrees.

8.0 CONCLUSIONS

The experiments conducted have shown the new rig to have little interference as compared to the old rig. The interference that is present should be greatly reduced by judicial attachment arrangements between the model and sting, as opposed to jubilee clips, and by keeping any wires from protruding into the flow. A firm basis has been established from which multi-body tests can be conducted.

It has been shown that the usual practice of applying a zero incidence shift as a correction to the normal force versus incidence and pitching moment versus incidence curves is valid, in the sense that it corrects the incidence at zero normal force and zero pitching moment, but does not give the correct values of slope. Because detailed pressure and load distribution data is available, as opposed to the usual overall force and moment data, it is possible to make a more precise correction.

The theoretical prediction technique, SPARV (inviscid), gives good results for the flow over the nose region, but the viscous extension does not give good agreement with experiment over the boattail, even with a higher number of viscous iterations. However, by the use of SPARV, in predicting the correction to the incidence, it has been shown how modern computer techniques and wind tunnel tests can compliment each other to present a better understanding of the characteristics of the flow around the body being tested, a point in case being the location of the centre of pressure (Sec.4.5).

It has been shown that the RING SOURCE method of, Ref.4, gives good agreement with inviscid SPARV, with a considerable saving in run time.

REFERENCES

1 PETRIE, J.H. SPARV user notes (Addendum to YAD 3382) BAe Brough.

2 CHRISTOPHER, P.A.T. SHAW, C.T. The use of source and doublet distributions in generating the lifting characteristics of axi-symmetric bodies:- boundary layer influence. C.I.T., Cranfield, College of Aeronautics Memo 8211 May 1982

3 CHRISTOPHER, P.A.T. SHAW, C.T. The subsonic aerodynamic characteristics of a body of revolution - comparison between theory and experiment, including the effects of model support interference. C.I.T., Cranfield, College of Aeronautics Report 8315 June 1983

4 CHRISTOPHER, P.A.T. DEO, H.S. SHAW, C.T. A ring source method for predicting the aerodynamic characteristics of bodies of revolution. C.I.T., Cranfield, College of Aeronautics Report 8409 March 1984

5 BIGNELL, P.R. The Aerodynamics of Guided Weapons - Body Aerodynamics. Section 4.2. C.I.T., Cranfield, College of Aeronautics Short Course Notes.

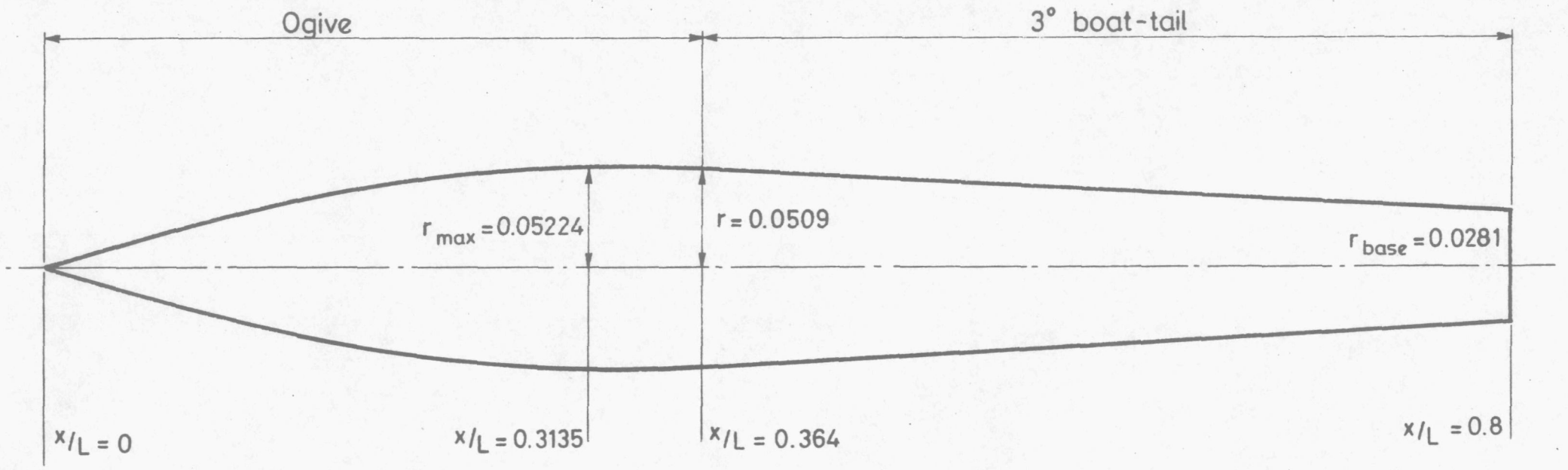

Figure 1. The model shape.

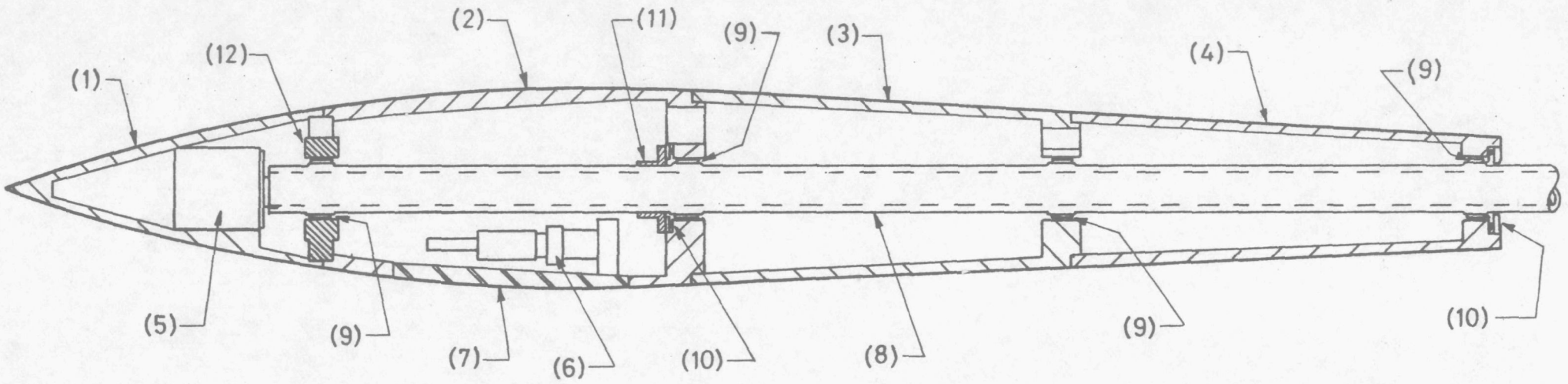

1. Nose section
2. Fore body section
3. Centre body section
4. Rear body section
5. Stepping motor
6. Scanivalve
7. Access hatch
8. Model centre tube
9. Needle radial bearing
10. Needle thrust bearing
11. Retaining nut
12. Bulk head flange

Figure 2. General assembly of model.

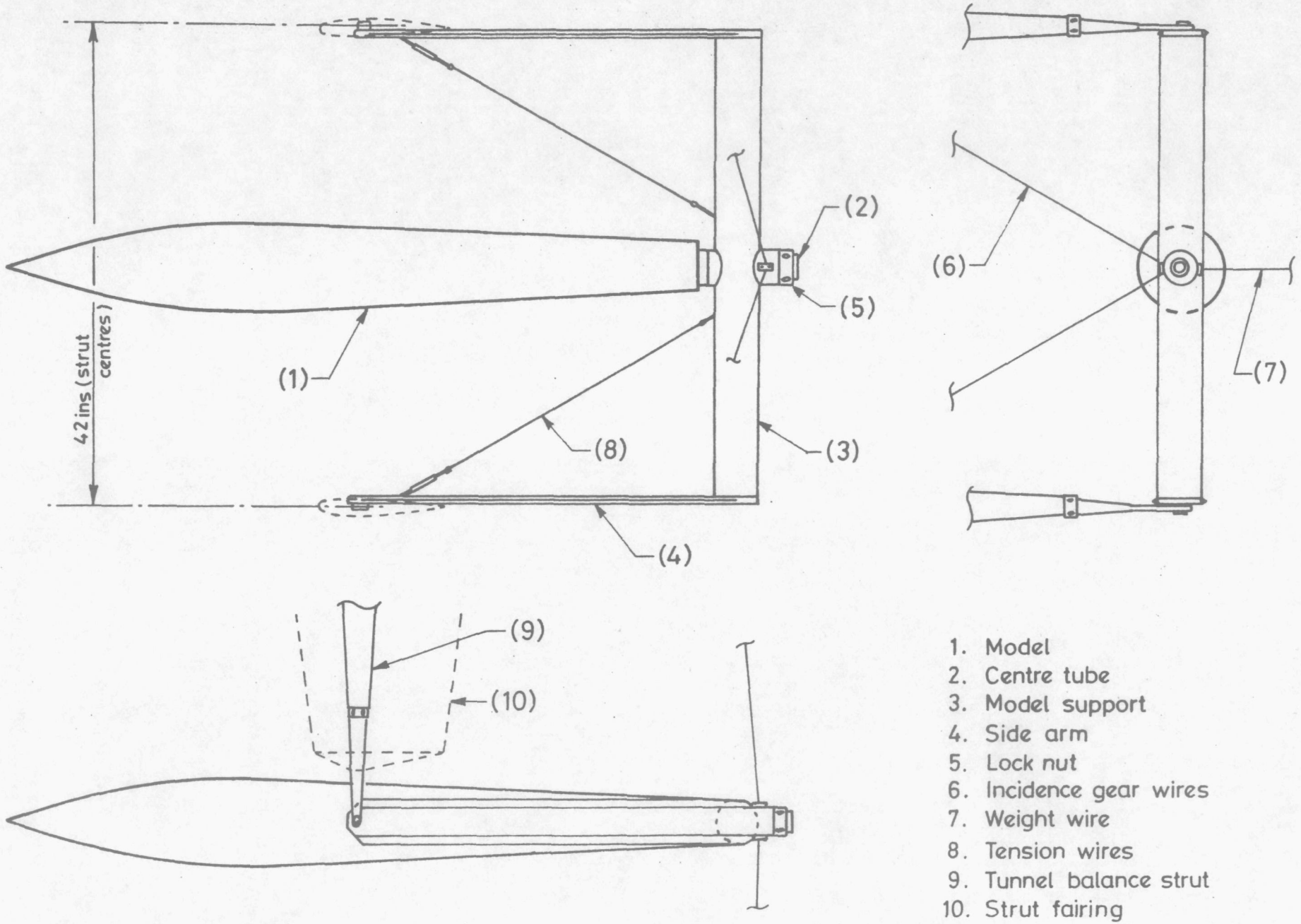

1. Model
2. Centre tube
3. Model support
4. Side arm
5. Lock nut
6. Incidence gear wires
7. Weight wire
8. Tension wires
9. Tunnel balance strut
10. Strut fairing

Figure 3. General assembly of old support rig.

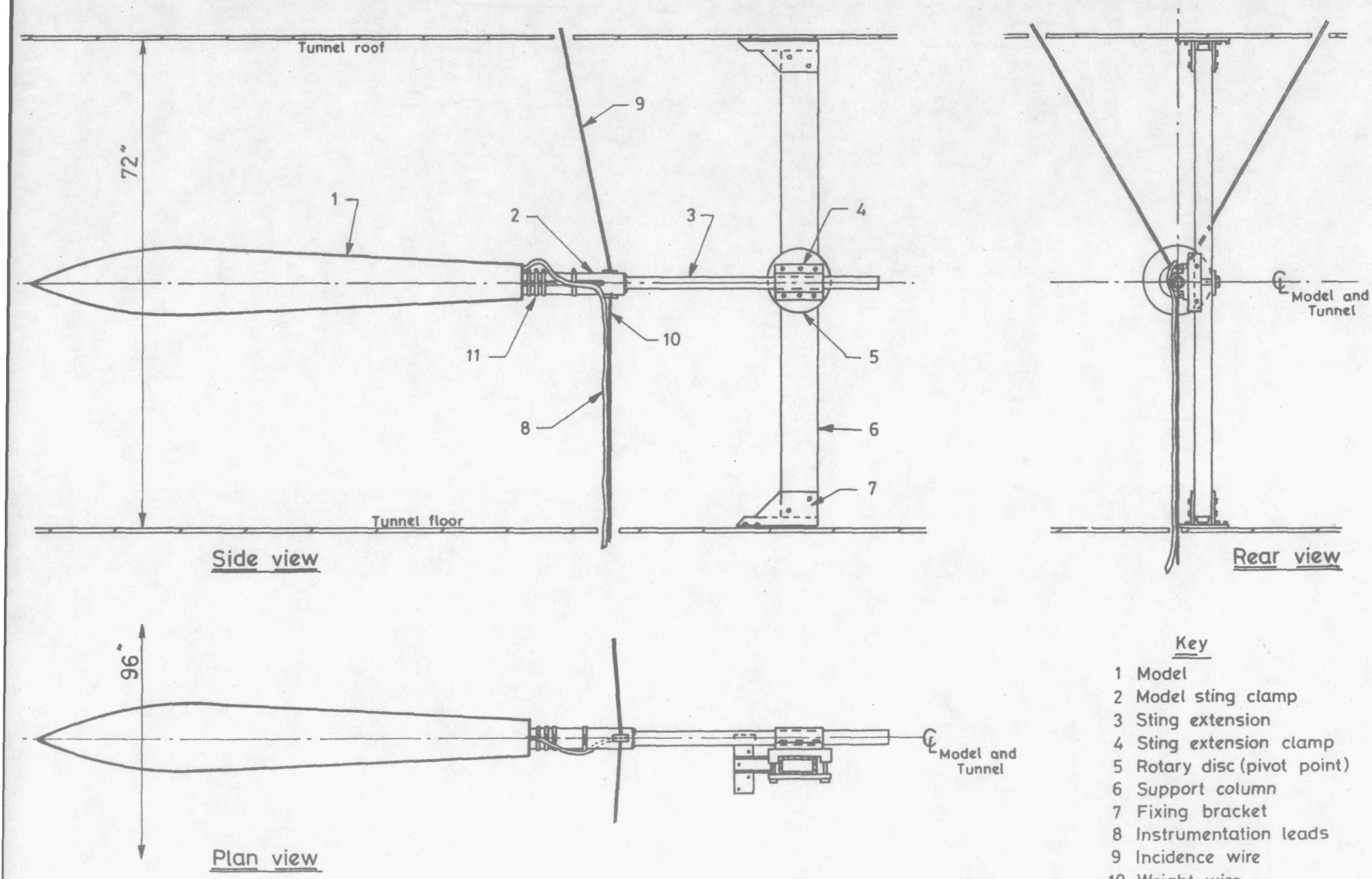

Fig. 4. General assembly of new support rig

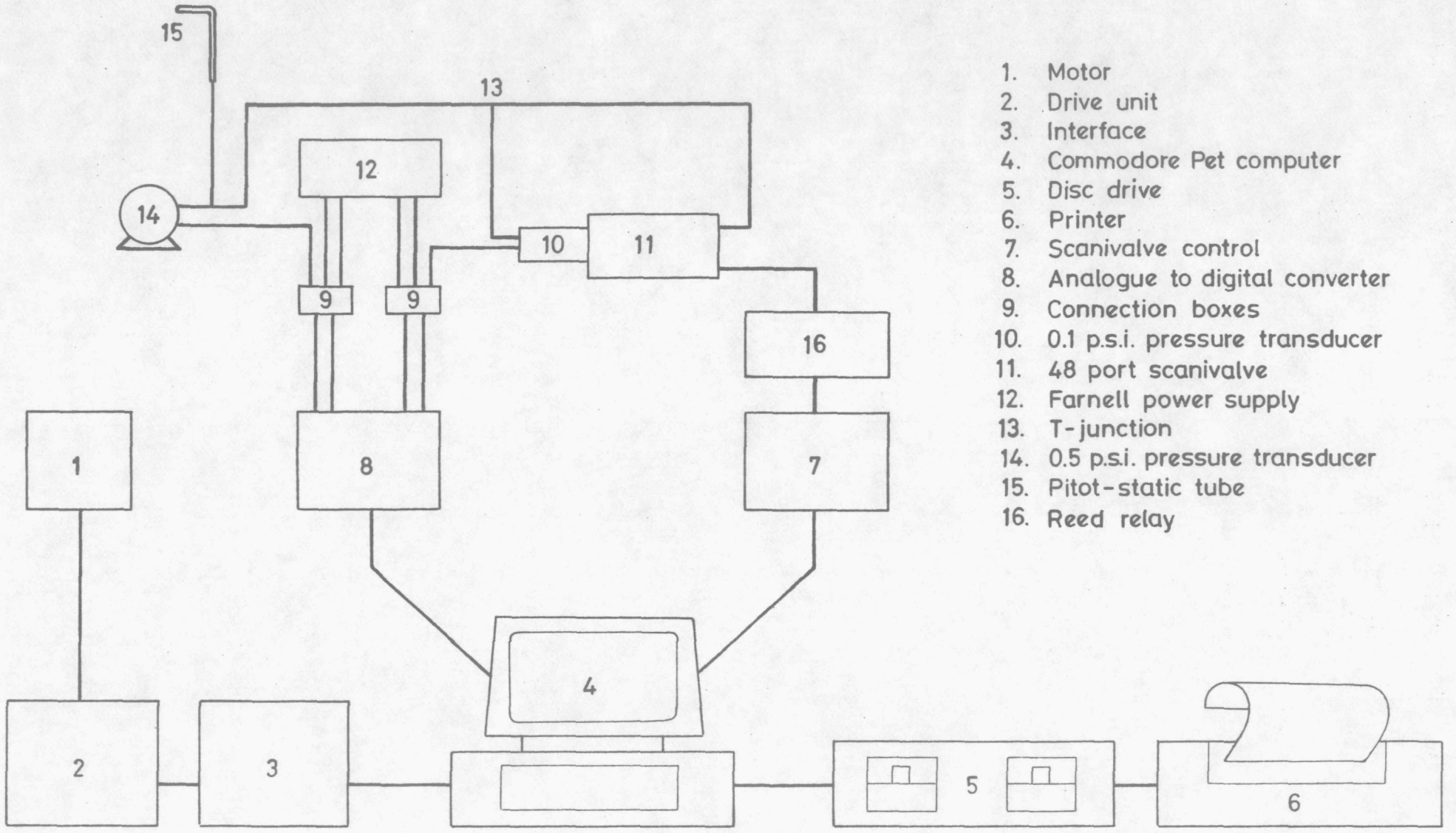

Fig.5. Schematic diagram of instrumentation.

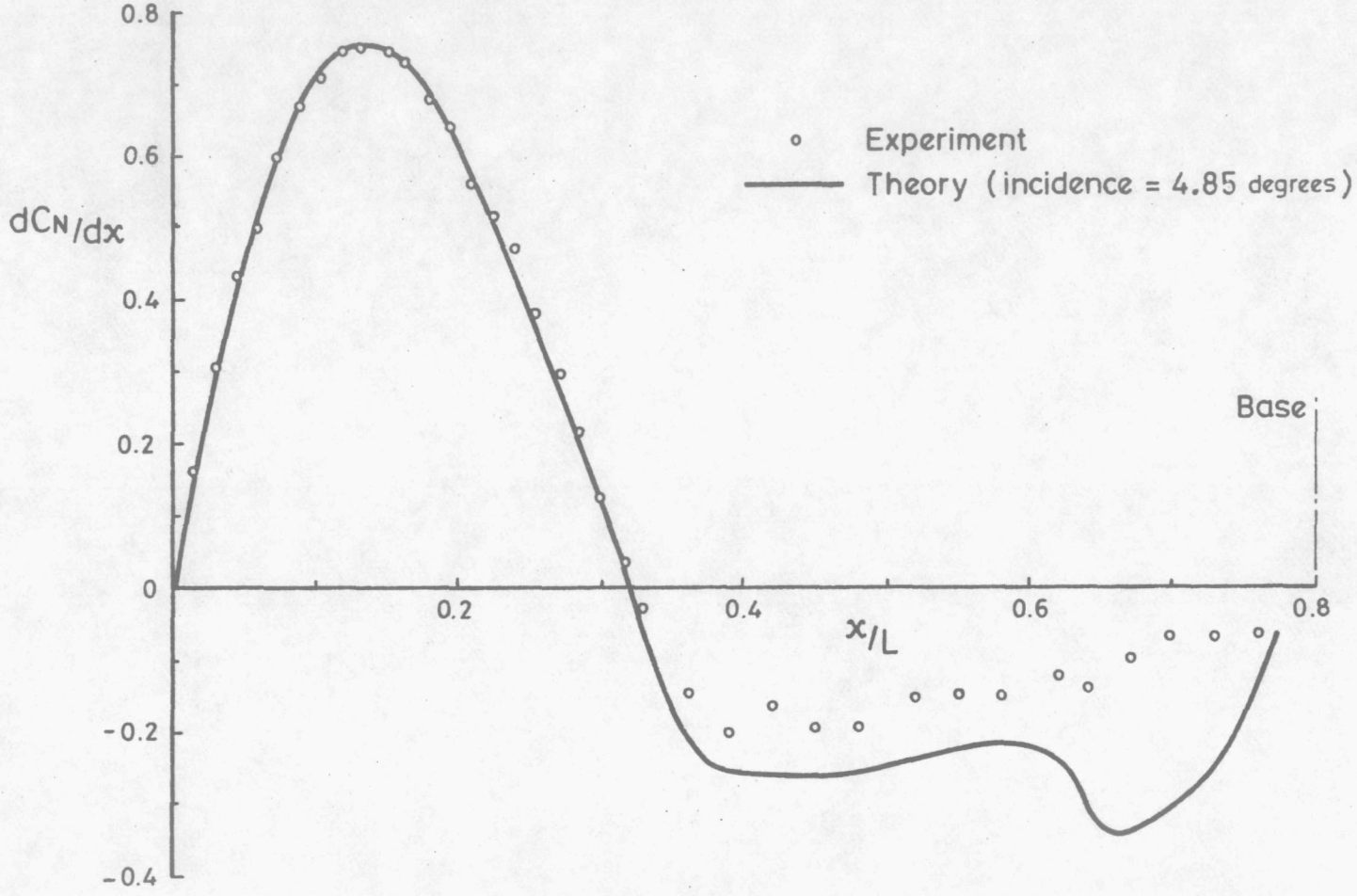

Figure 6. Load distribution at 5° incidence.

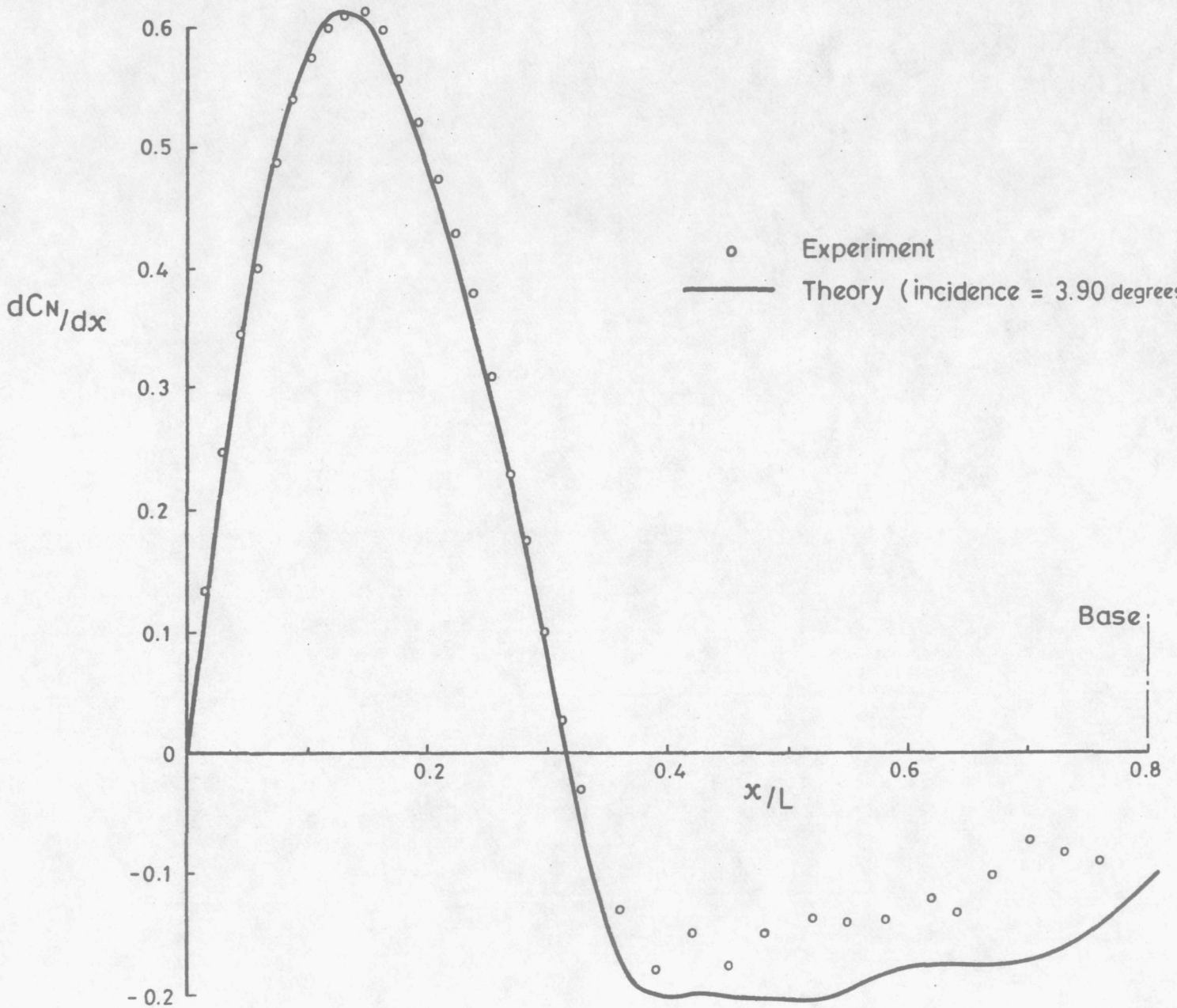

Figure 7. Load distribution at 4° incidence.

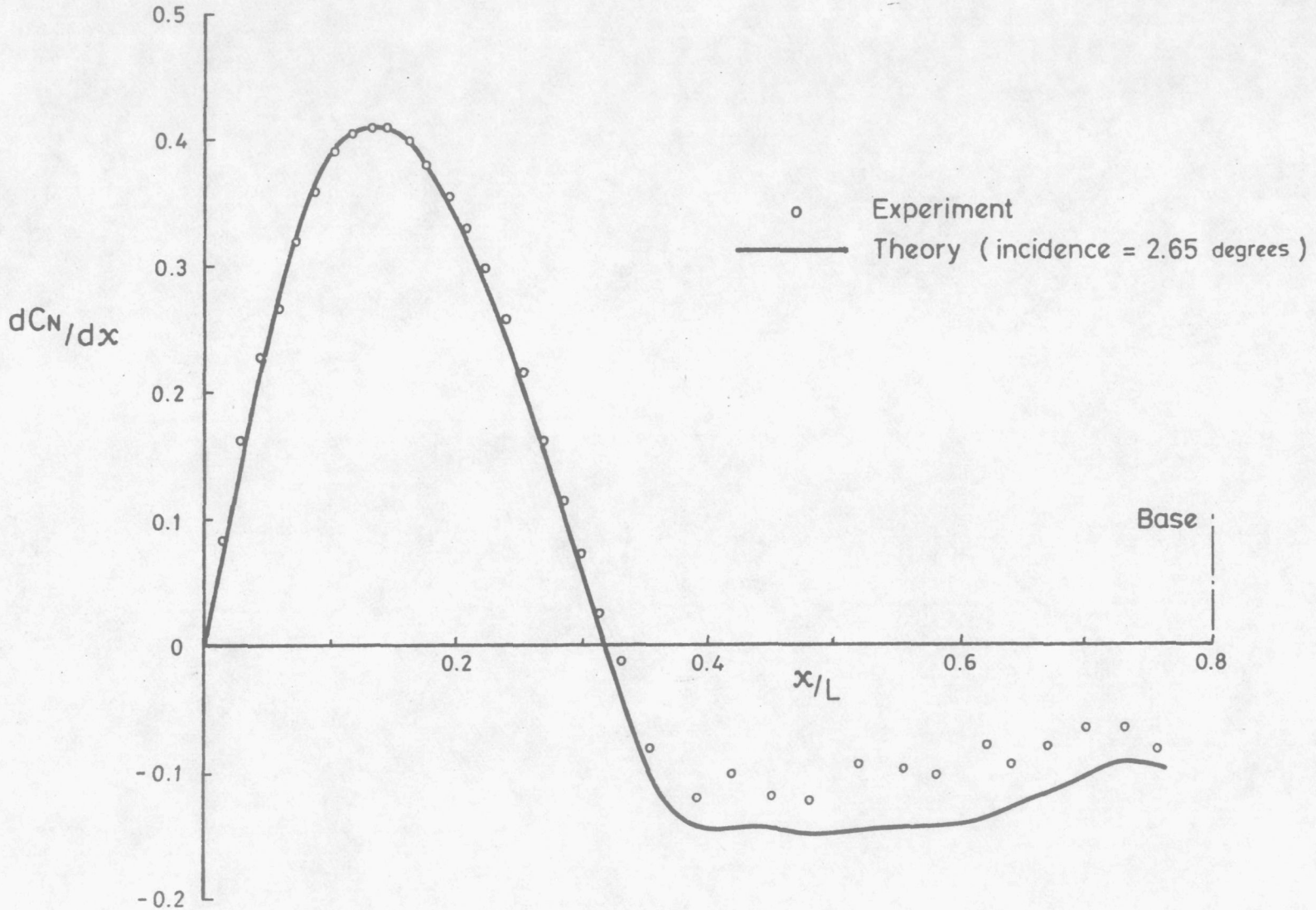

Figure 8. Load distribution at 3° incidence.

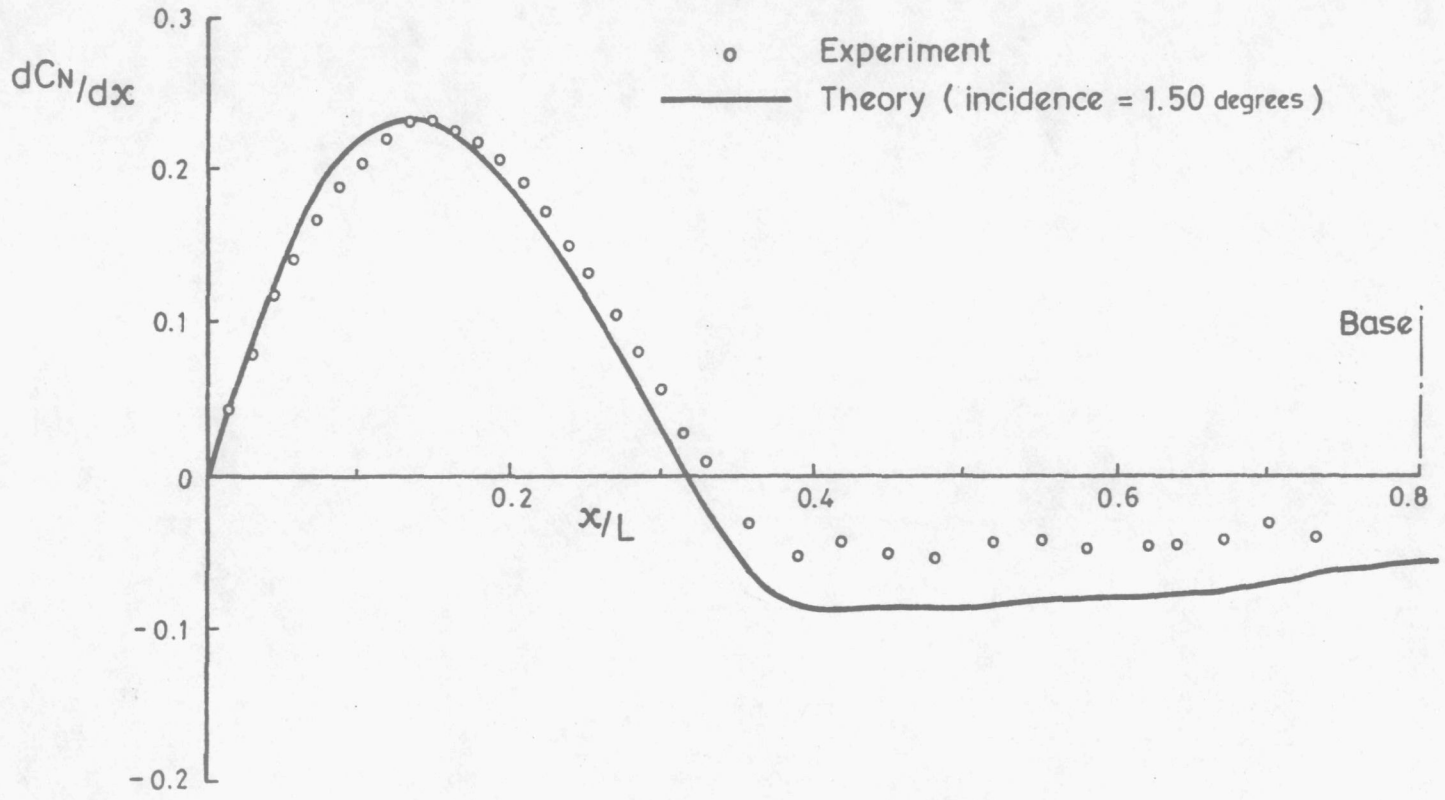

Figure 9. Load distribution at 2° incidence.

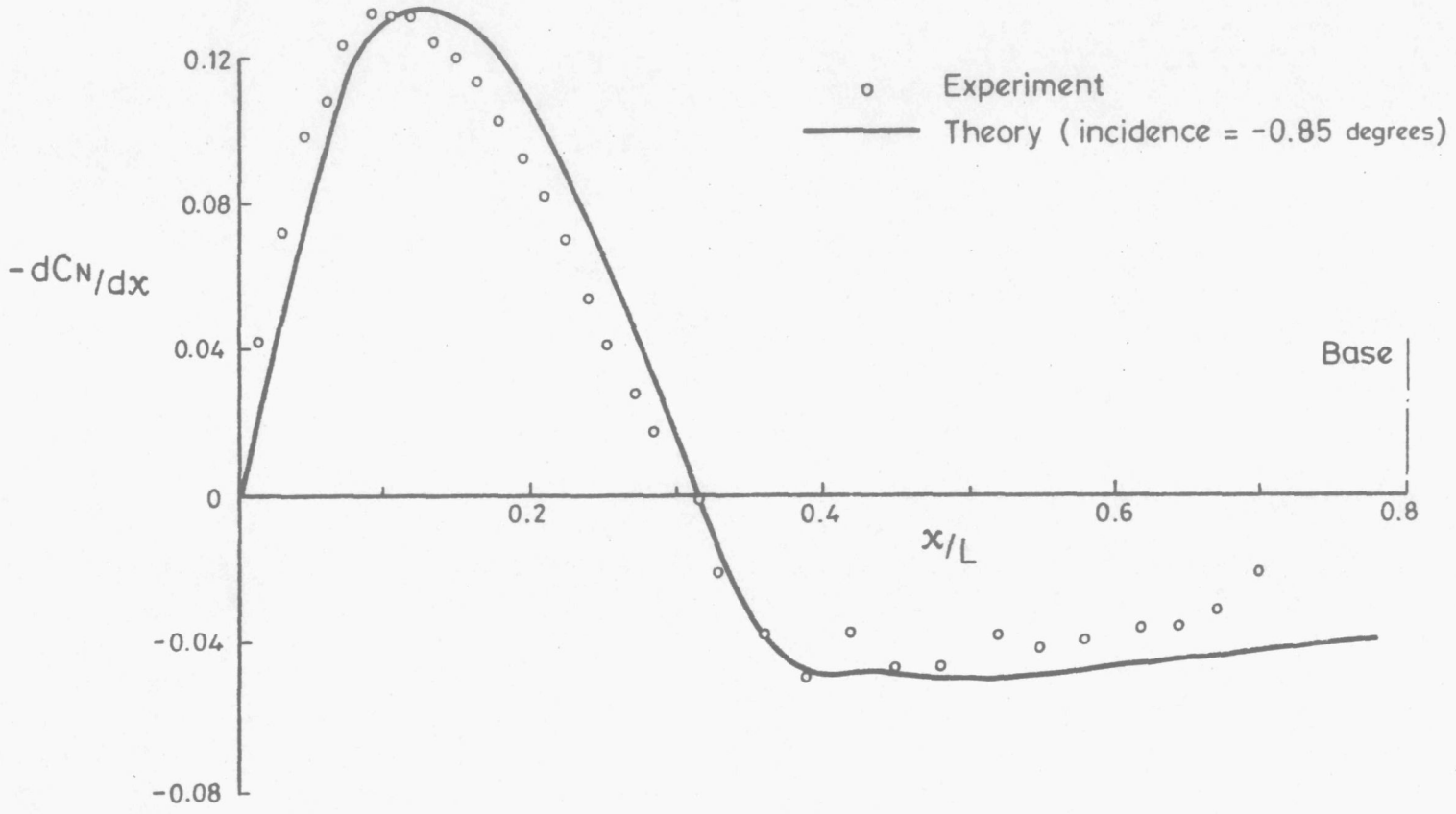

Figure 10. Load distribution at 0° incidence.

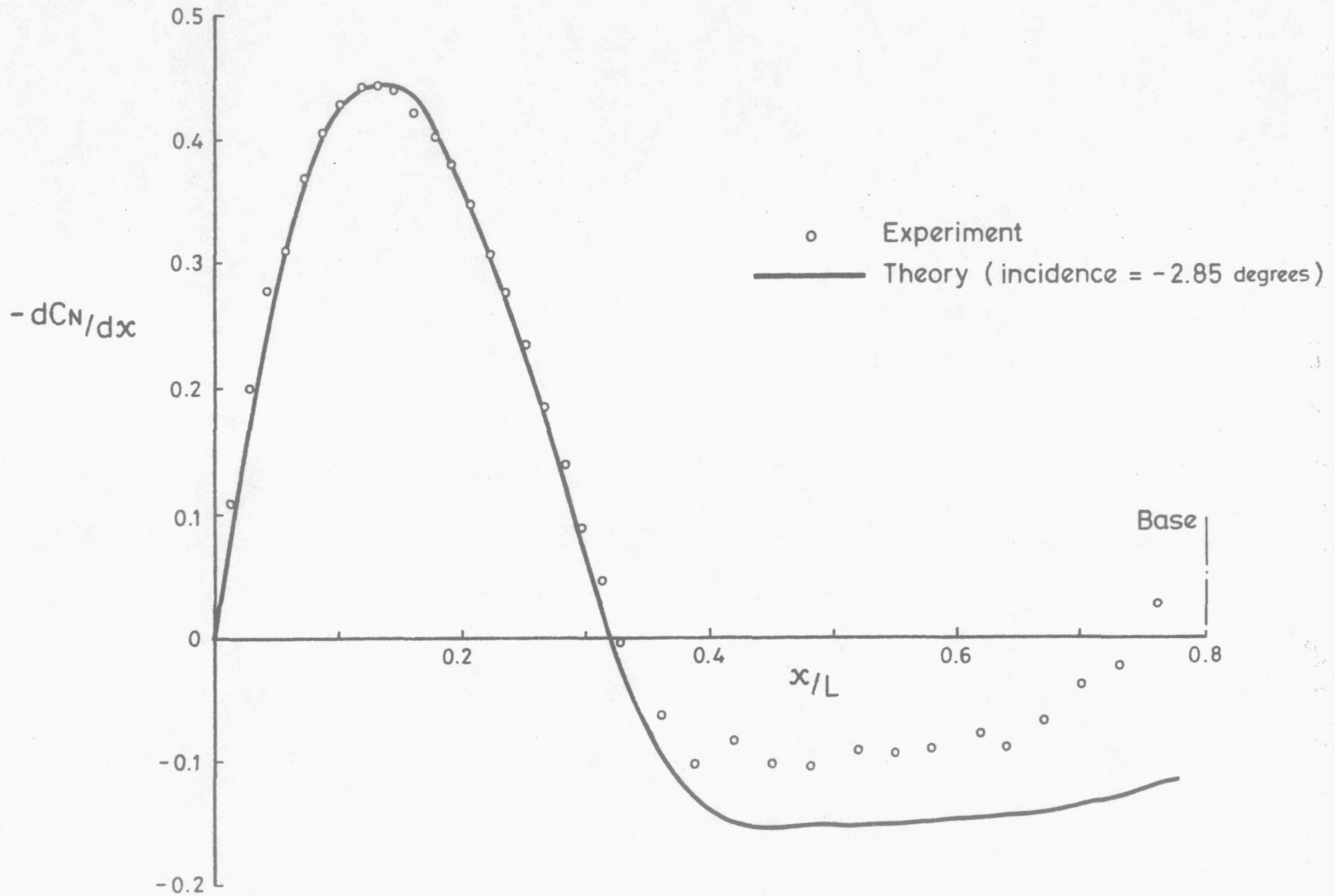

Figure 11. Load distribution at -2° incidence.

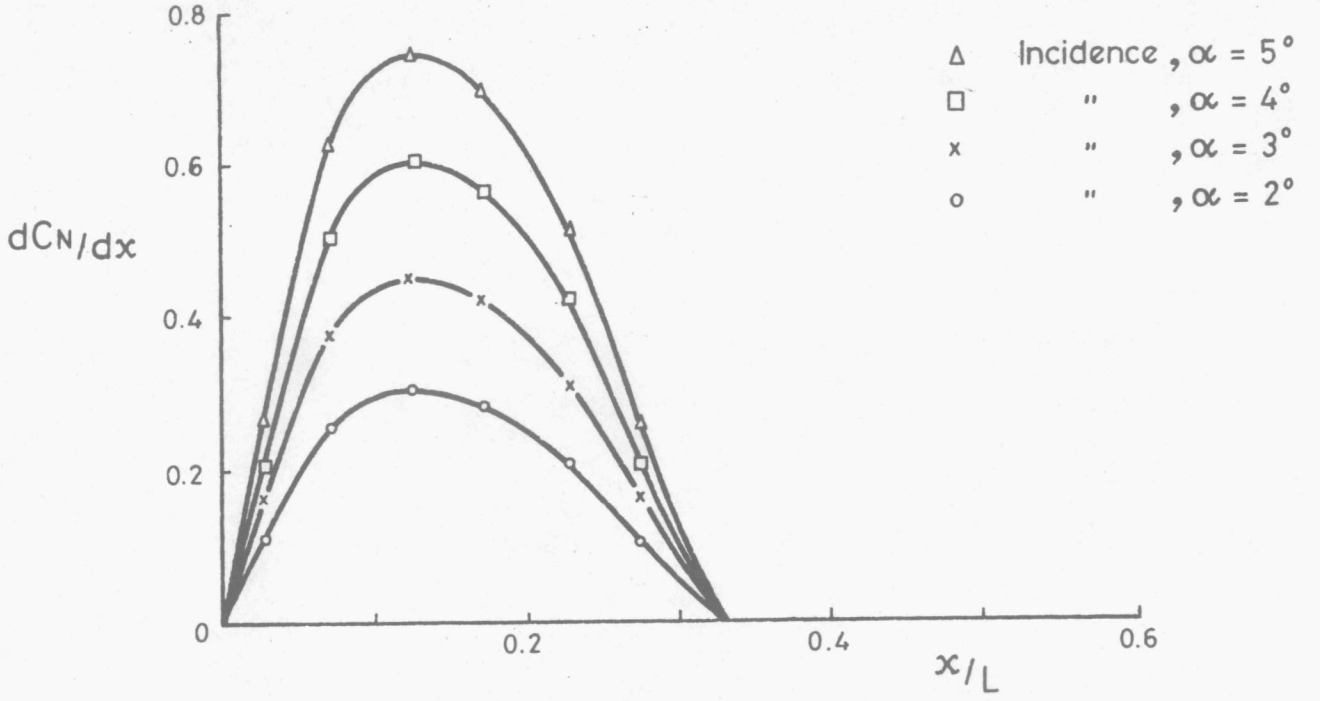

Figure 12. Nose-loading - Sparv (inviscid) - including back strut.

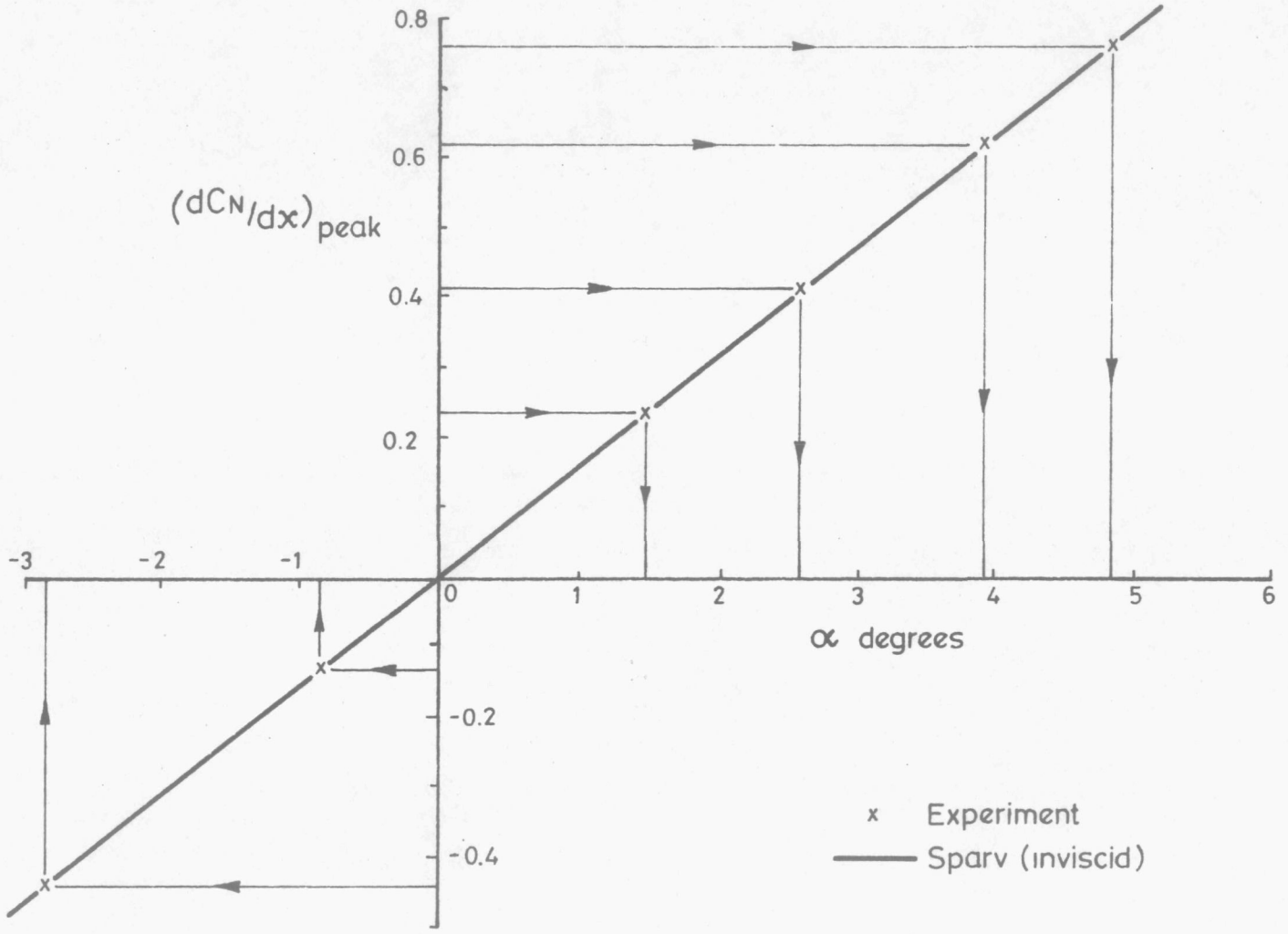

Figure 13. Correction to measured angle of incidence.

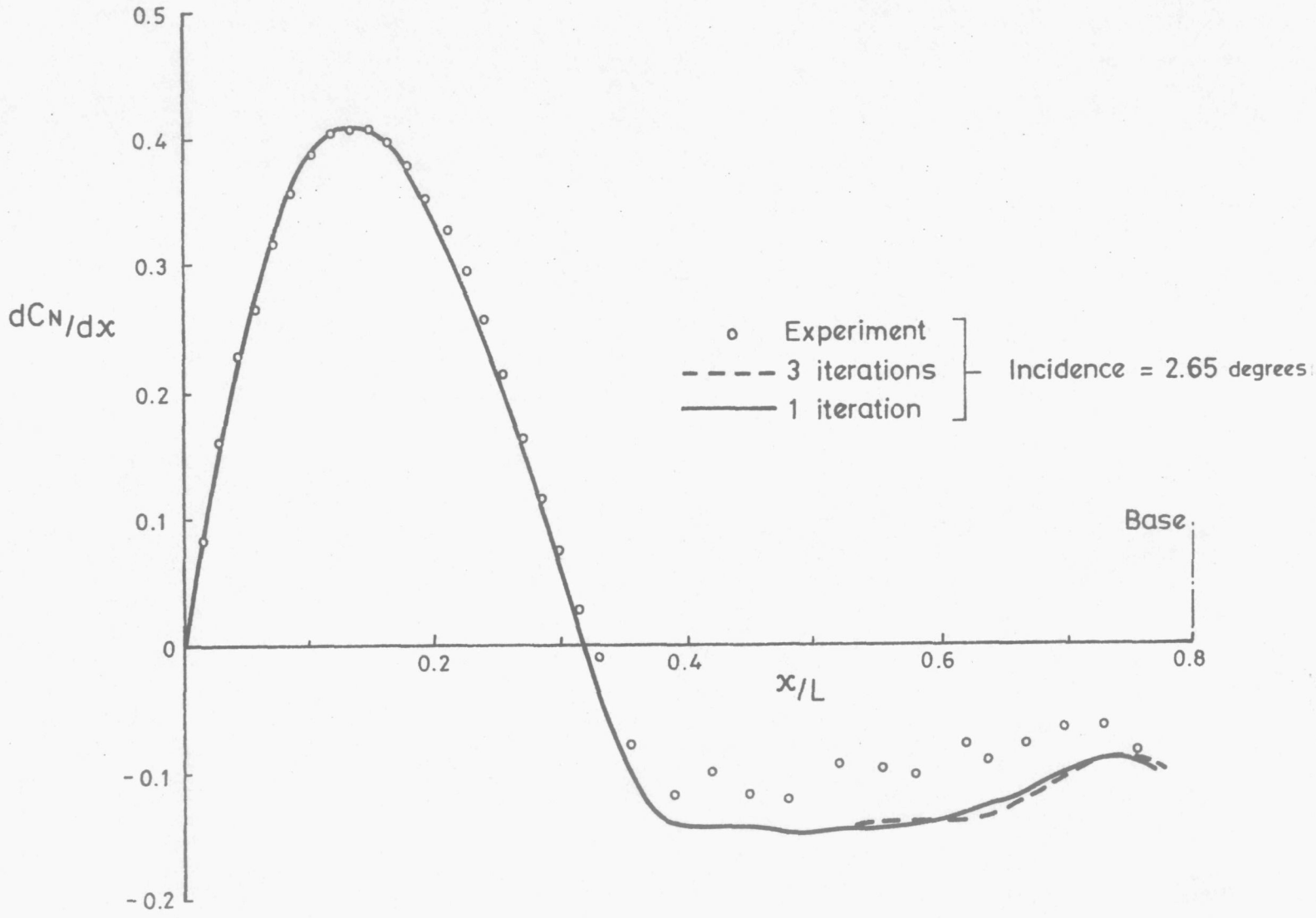

Figure 14. Comparison between viscous Sparv solutions.

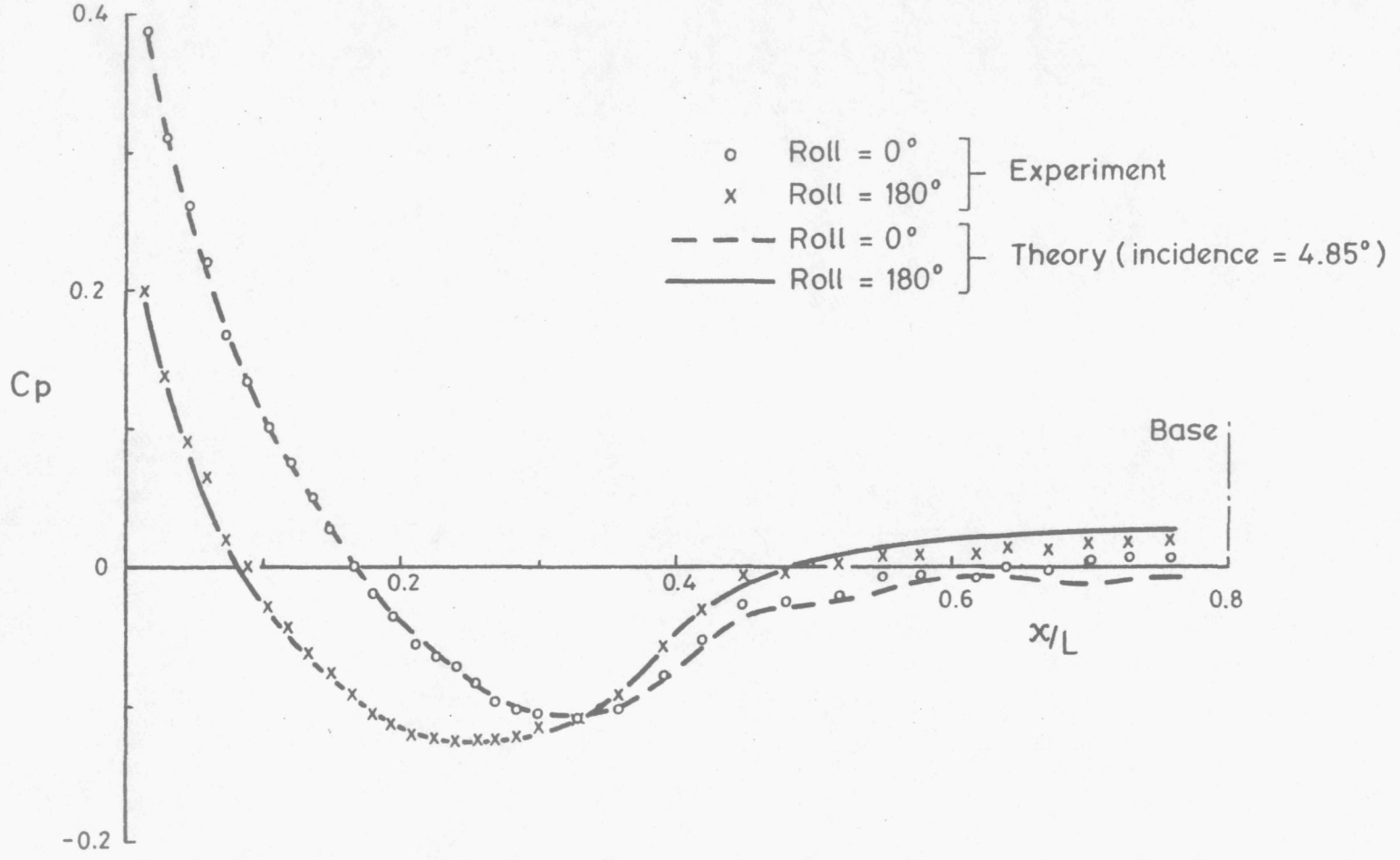

Figure 15. Pressure distribution at 5° incidence.

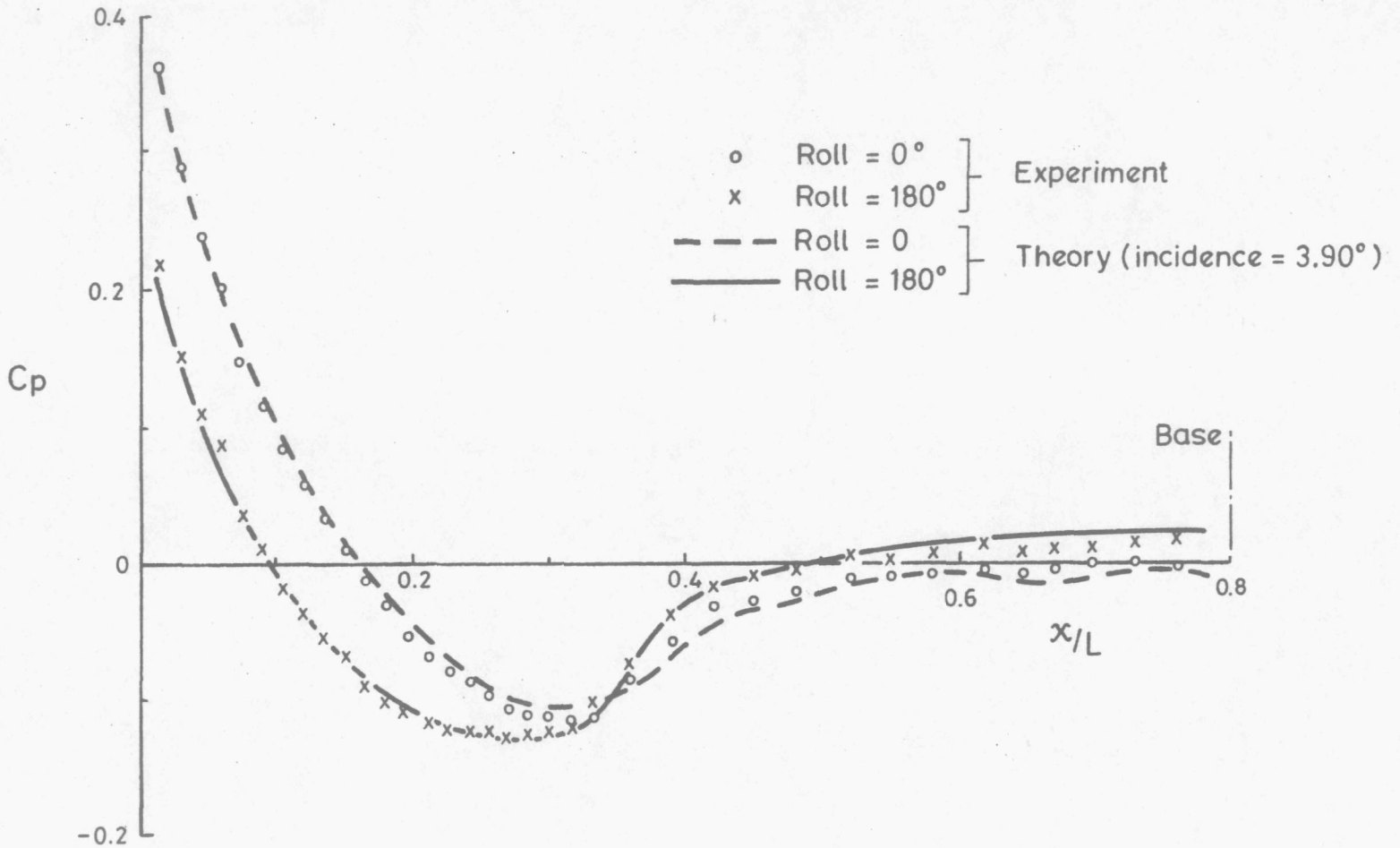

Figure 16. Pressure variation across roll angle at 4° incidence.

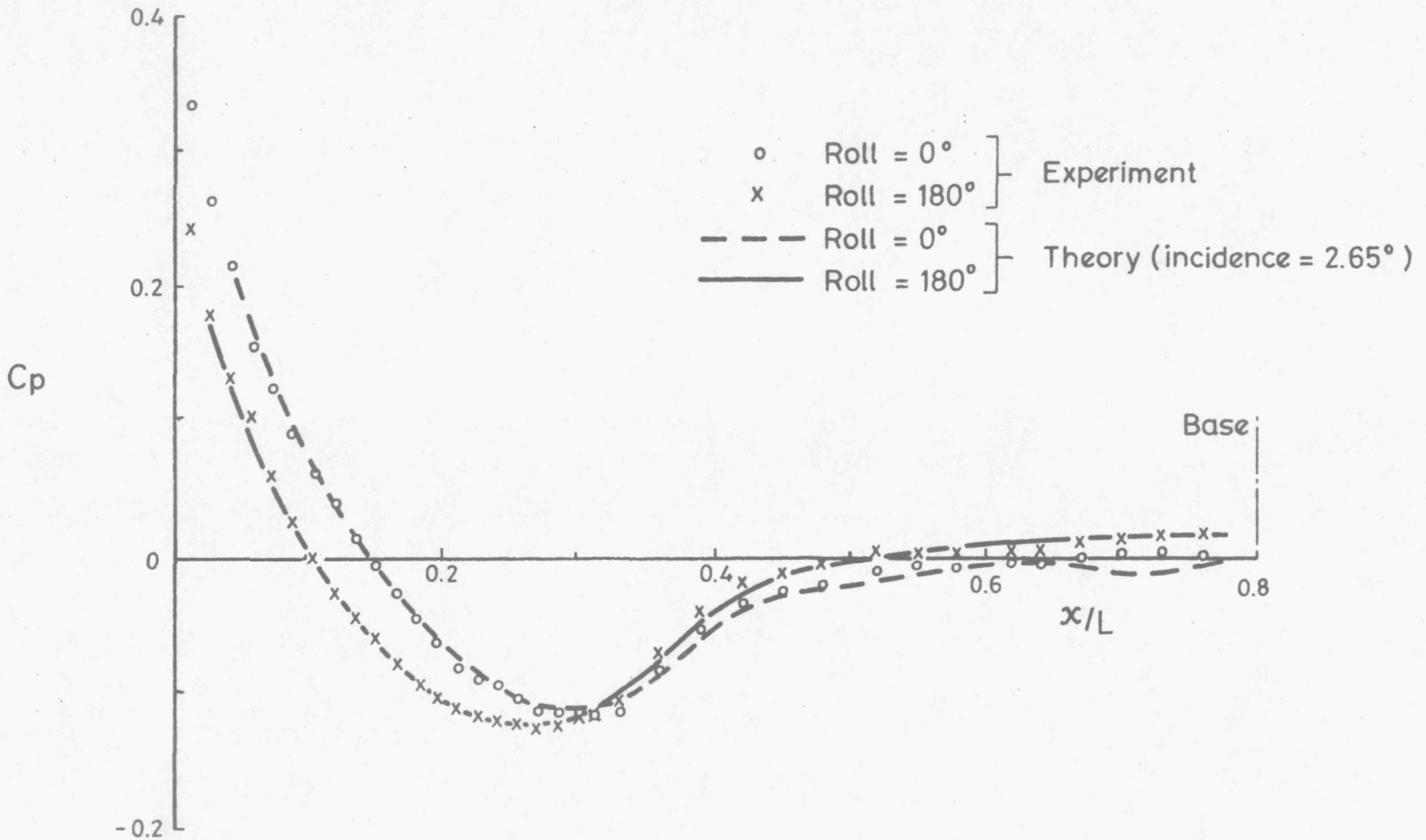

Figure 17. Pressure variation across roll angle at 3° incidence.

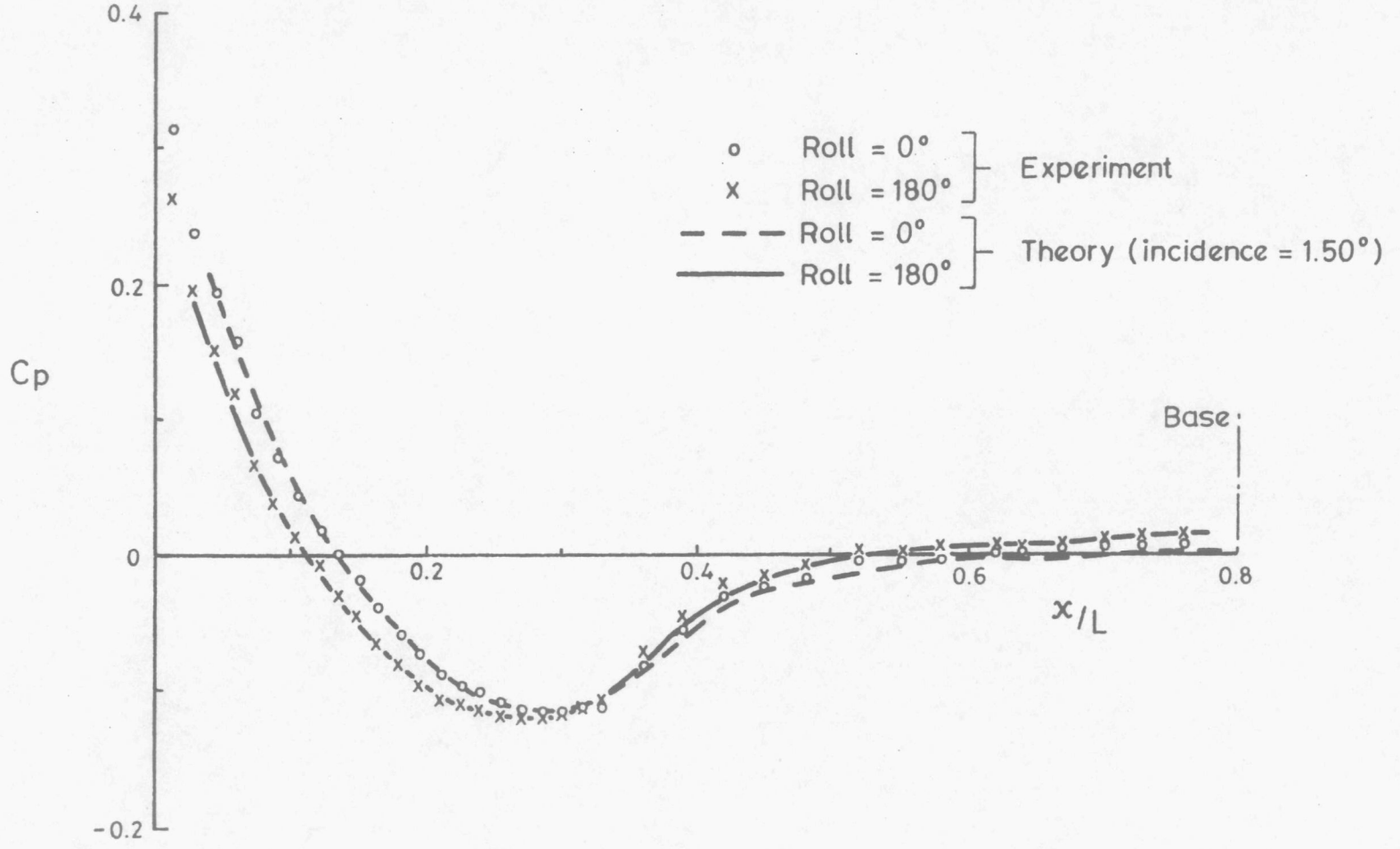

Figure 18. Pressure variation across roll angle at 2° incidence.

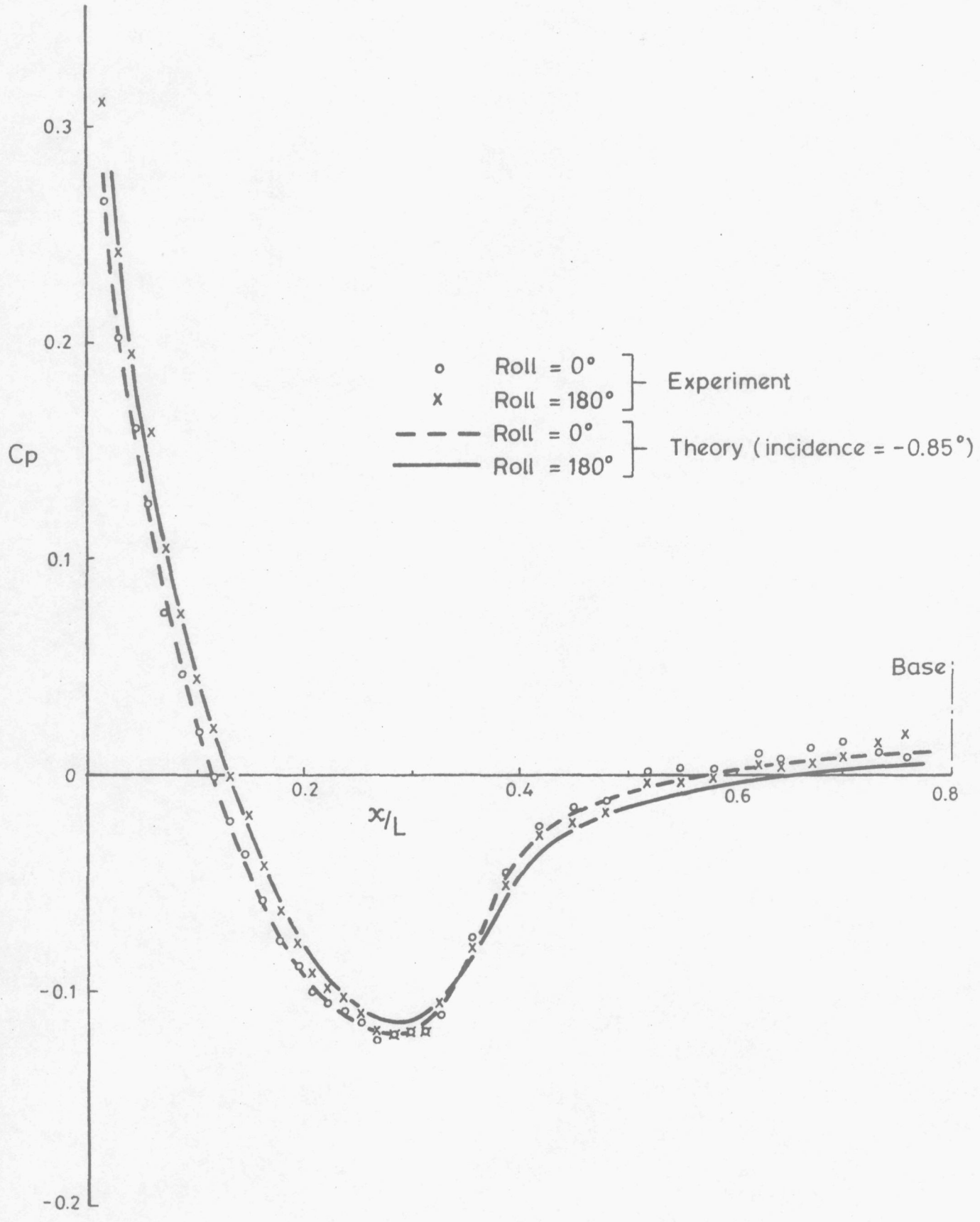

Figure 19. Pressure variation across roll angle at 0° incidence.

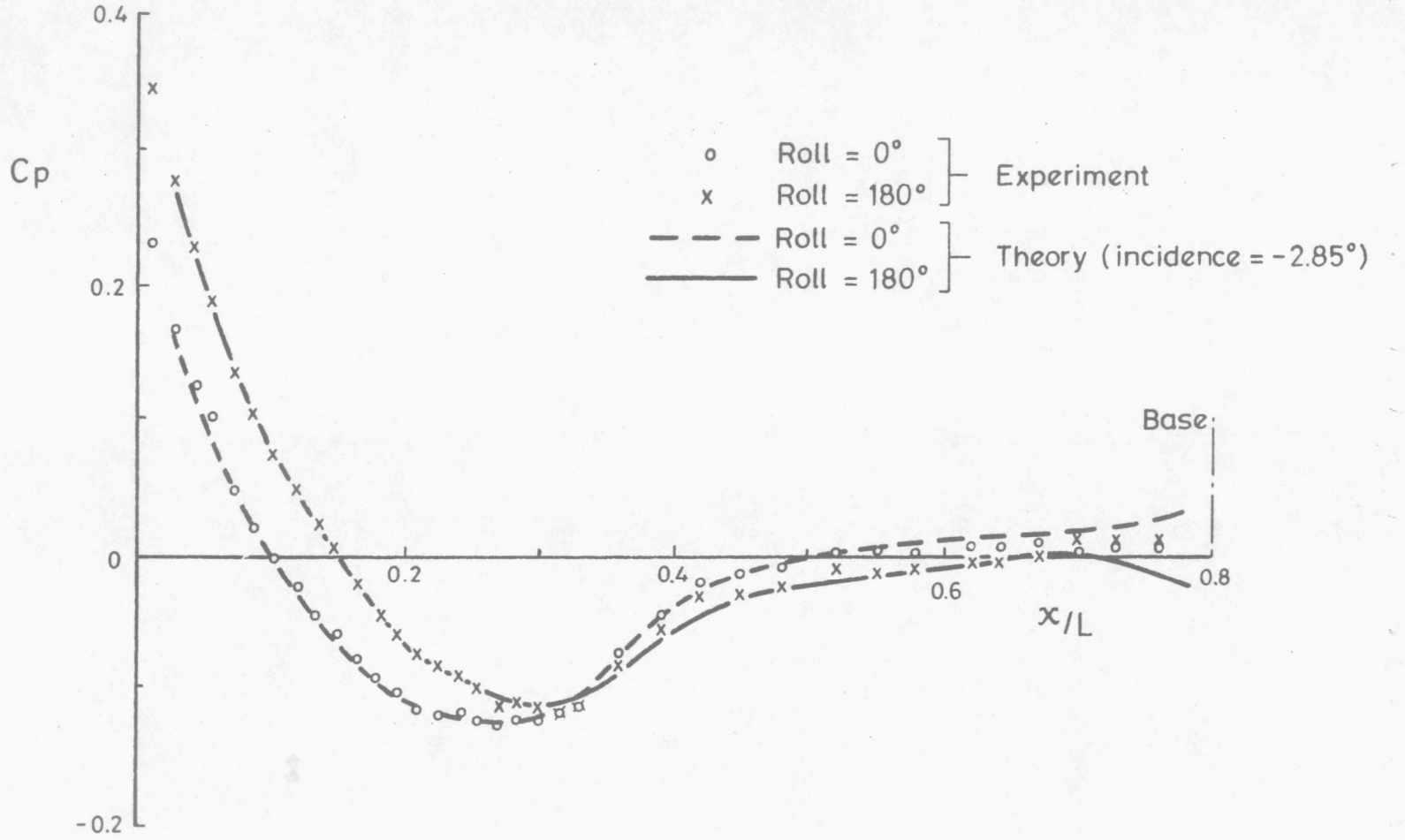

Figure 20. Pressure variation across roll angle at -2° incidence.

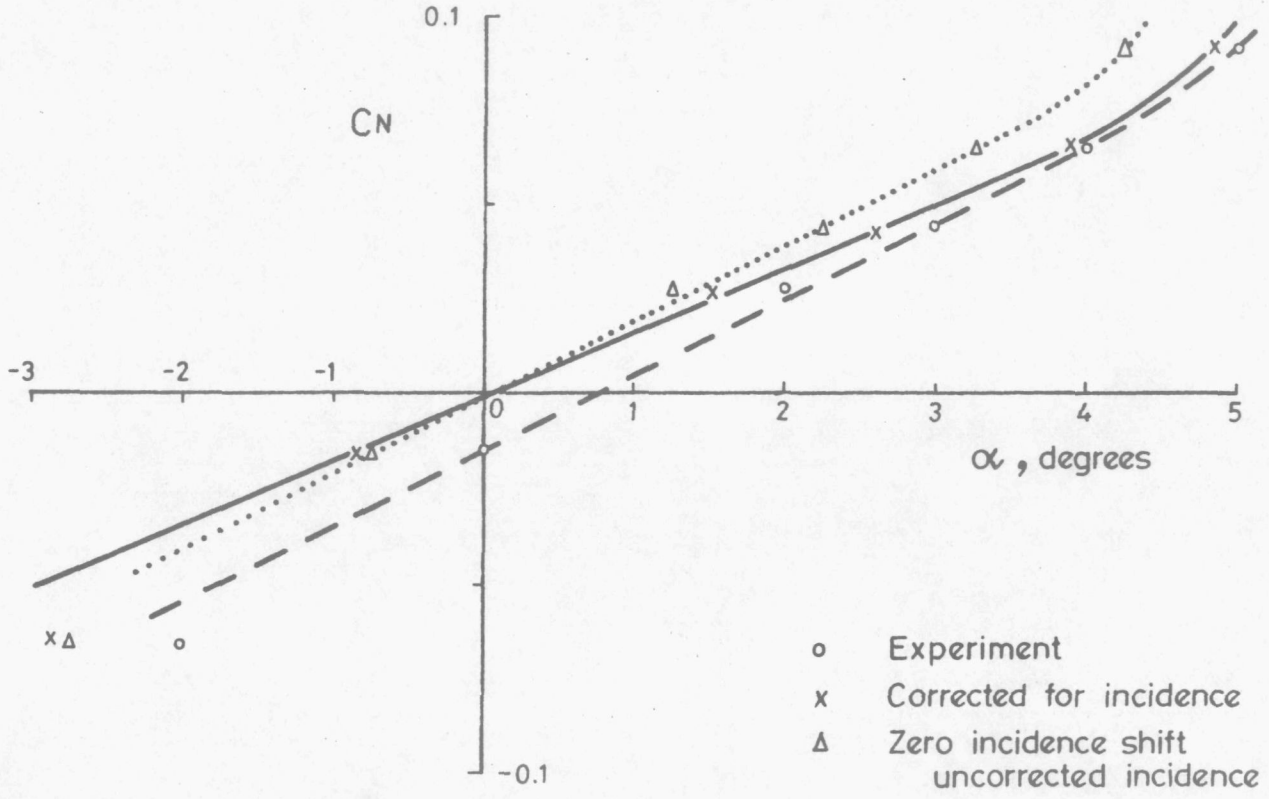

Figure 21. Normal force coefficient variation with incidence.

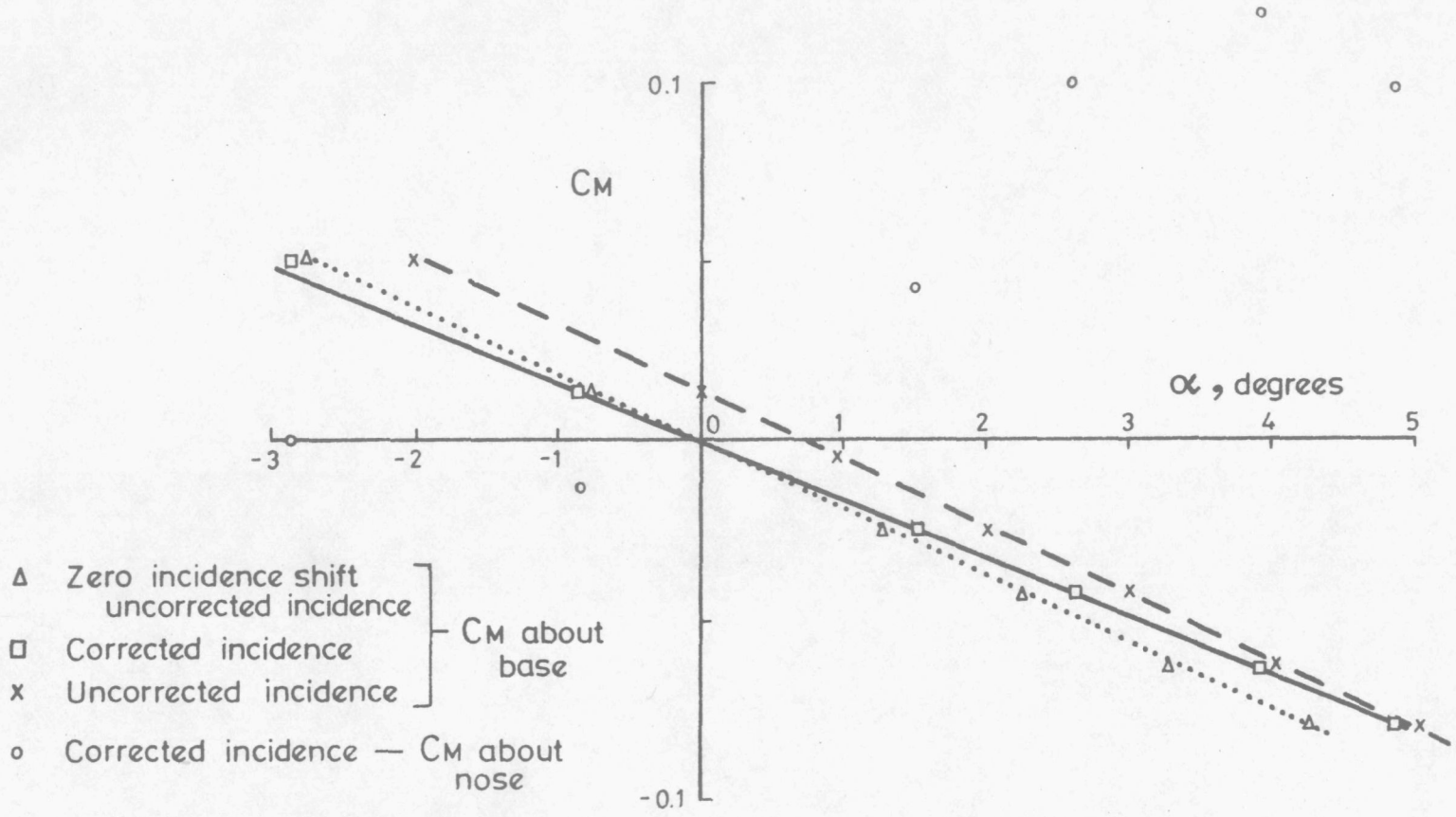

Figure 22. Pitching moment coefficient variation with incidence.

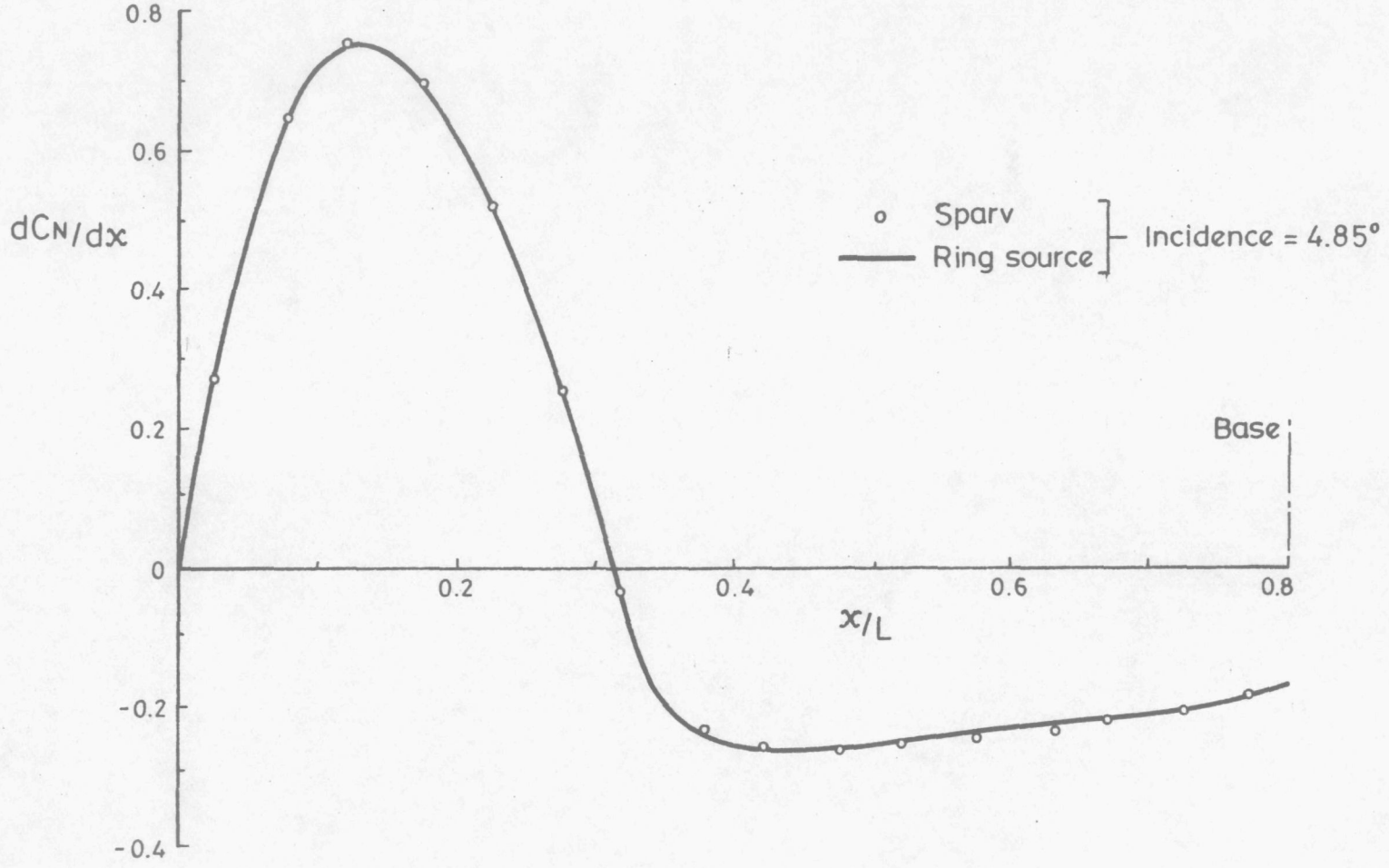

Figure 23. Comparison between inviscid Sparv and ring source method.

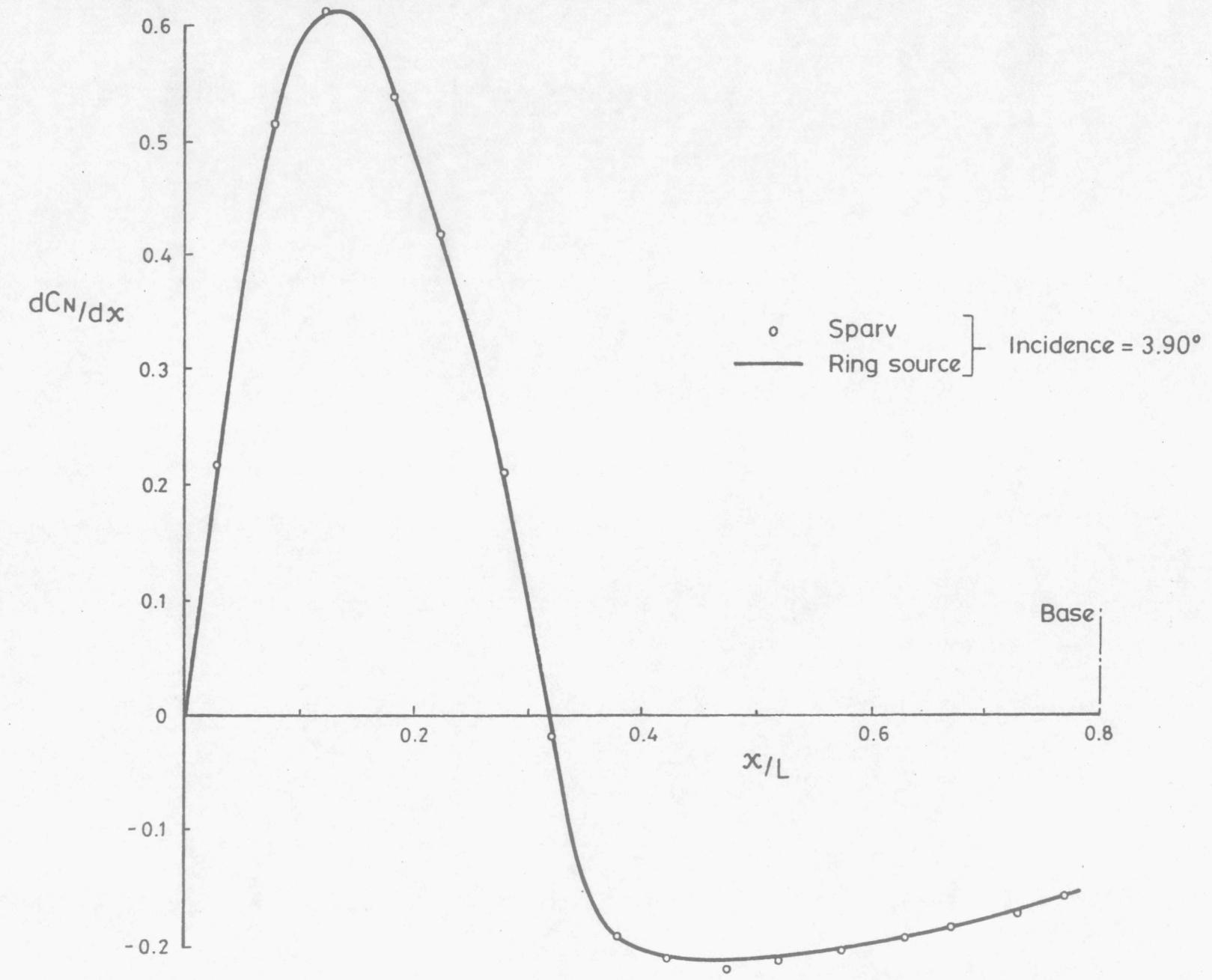

Figure 24. Comparison between inviscid Sparv and ring source method.

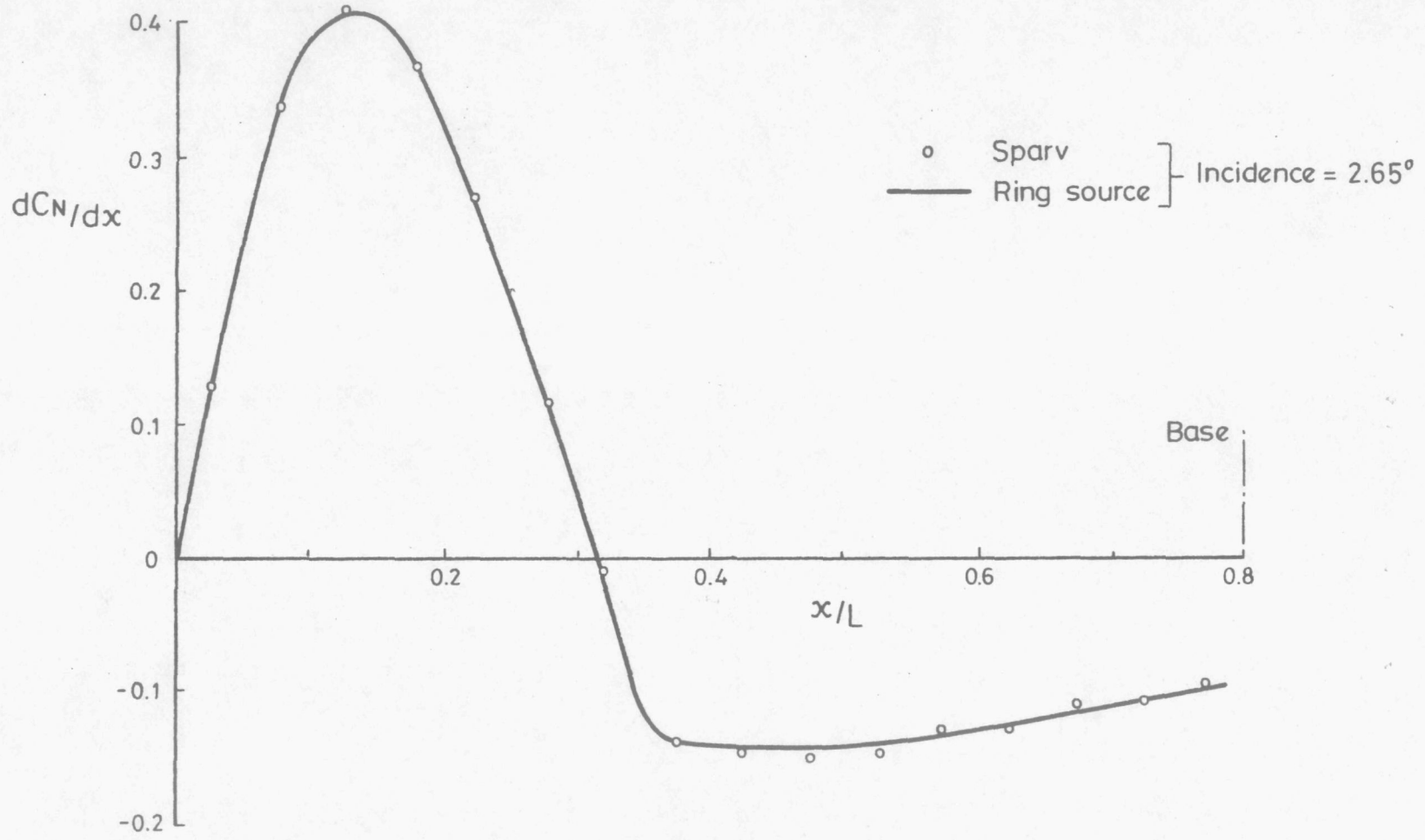

Figure 25. Comparison between inviscid Sparv and ring source method.

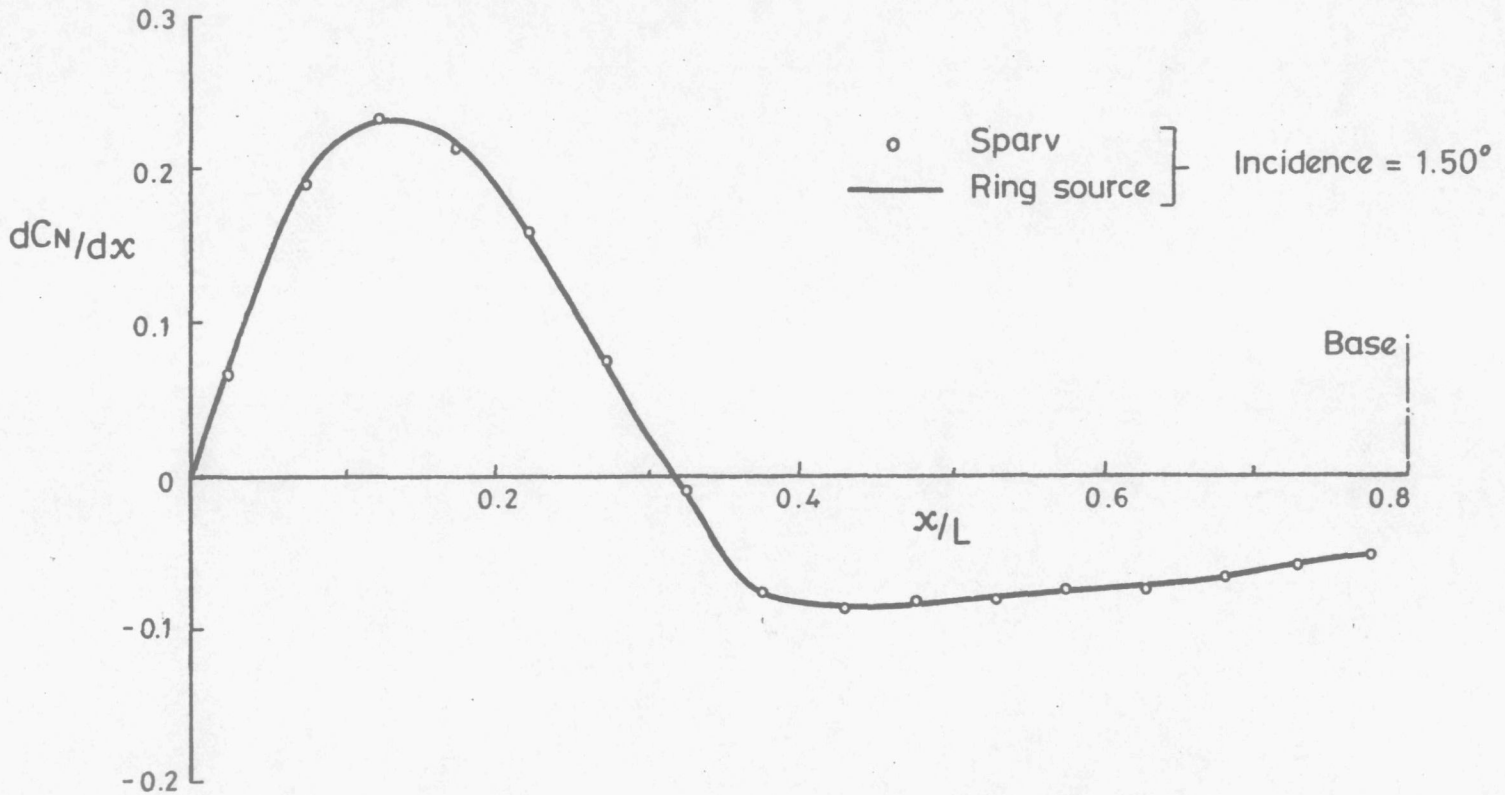

Figure 26. Comparison between inviscid Sparv and ring source method.

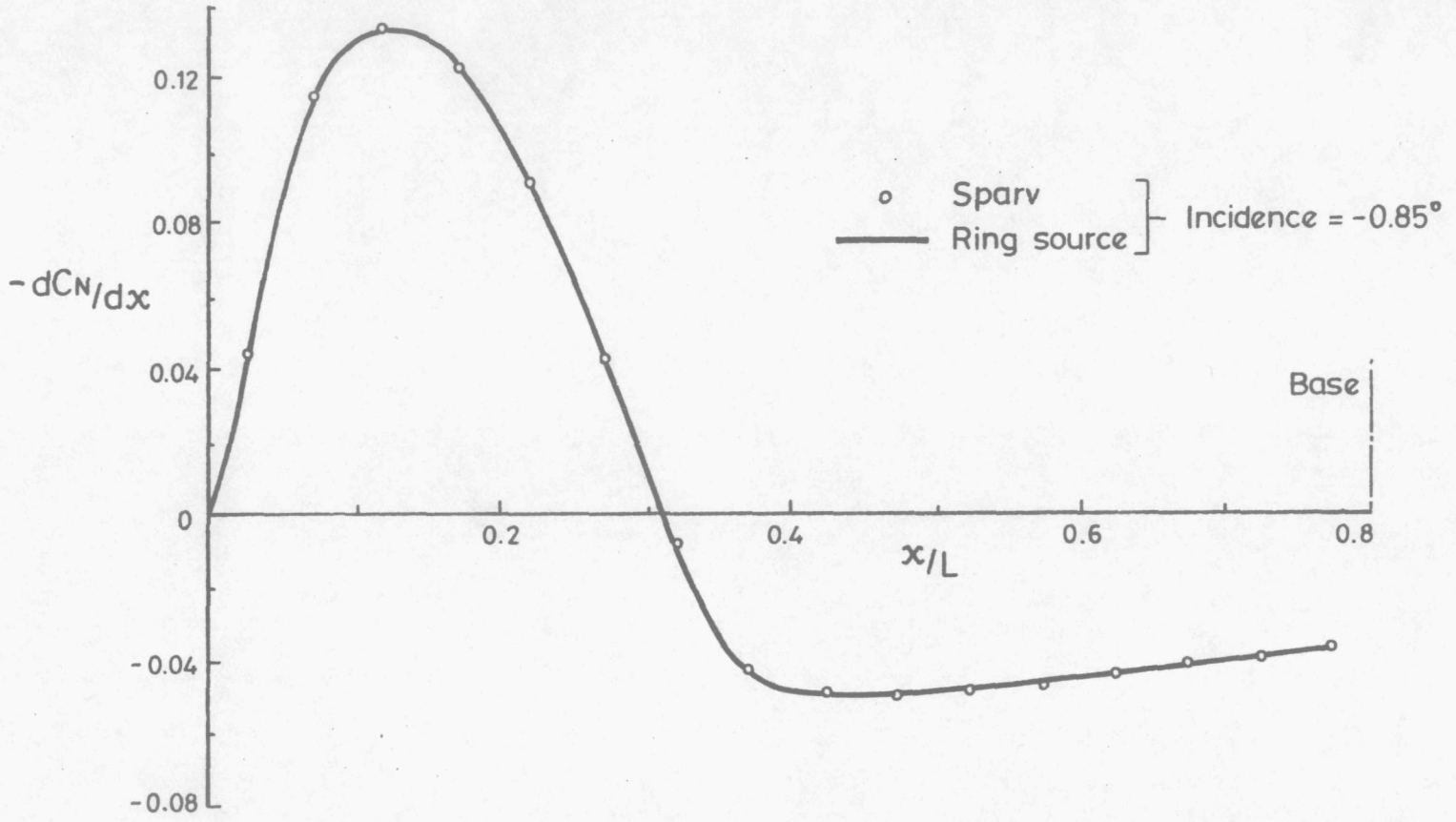

Figure 27. Comparison between inviscid Sparv and ring source method.

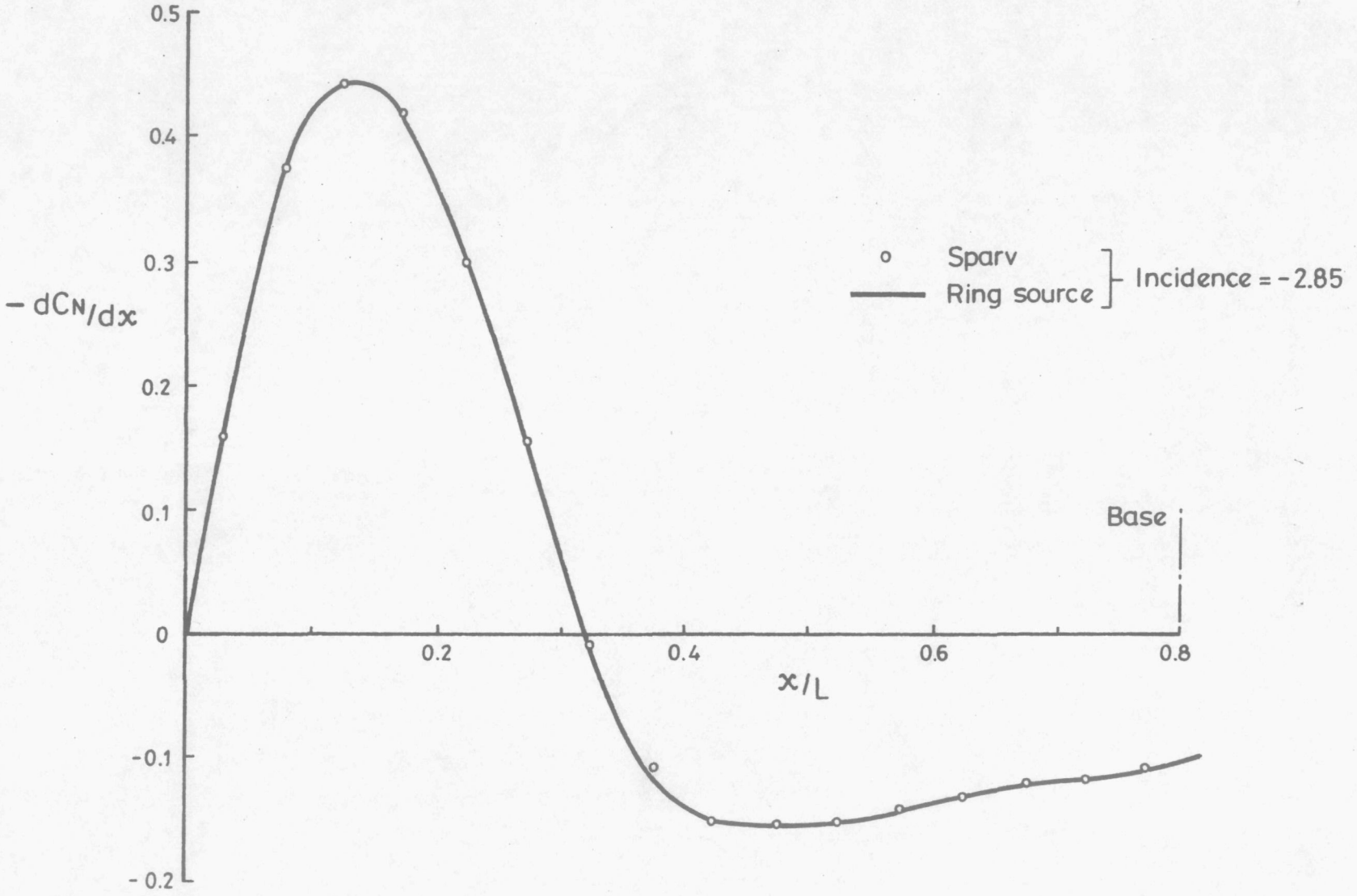

Figure 28. Comparison between inviscid Sparv and ring source method.

APPENDICES

APPENDIX.A.

CENTRE OF PRESSURE LOCATION.

- EXPERIMENTAL and SEMI-EMPIRICAL RESULTS.

Note: X_{cp} is in calibres ahead of the nose.

ALP	Cn_e	Cn_b	Cm_e	Cm_b	Xcp_e	Xcp_b
-2.85	-0.066	-0.074	0.503	0.065	0.003	0.869
-0.85	-0.014	-0.024	0.122	0.030	0.918	1.242
1.50	0.028	0.048	-0.256	-0.077	1.570	1.600
2.65	0.044	0.089	-0.433	-0.156	2.270	1.750
3.95	0.066	0.139	-0.634	-0.265	1.909	1.903
4.85	0.092	0.177	-0.805	-0.355	1.057	2.001

Table.A.

ALP = Incidence in degrees.
Cn_e = Normal force coefficient - experimental.
Cn_b = Normal force coefficient - Brebner.
Cm_e = Pitching moment coefficient - experimental.
Cm_b = Pitching moment coefficient - Brebner.
Xcp_e = Centre of pressure location - experimental.
Xcp_b = Centre of pressure location - Brebner.

APPENDIX.B.

PRESSURE COEFFICIENT - EXPERIMENTAL RESULTS.

Note: Angle of incidence and angle of roll in degrees.

PRESSURE COEFFICIENT

INCIDENCE= 5

ROLL ANGLE

X/L	0	18	36	54	72	90	108	126	144	162	180
.015	+.386	+.374	+.351	+.320	+.287	+.257	+.231	+.212	+.203	+.199	+.196
.030	+.310	+.301	+.281	+.252	+.221	+.192	+.167	+.150	+.139	+.134	+.132
.045	+.262	+.250	+.230	+.206	+.178	+.149	+.126	+.107	+.098	+.092	+.090
.060	+.219	+.211	+.194	+.169	+.143	+.119	+.099	+.083	+.075	+.069	+.065
.075	+.165	+.159	+.142	+.118	+.092	+.068	+.047	+.032	+.023	+.018	+.017
.090	+.133	+.127	+.110	+.090	+.065	+.041	+.020	+.006	-.003	-.006	-.007
.105	+.100	+.094	+.079	+.059	+.035	+.012	-.005	-.019	-.026	-.030	-.031
.120	+.074	+.070	+.055	+.036	+.015	-.006	-.024	-.037	-.045	-.047	-.048
.135	+.048	+.044	+.030	+.011	-.010	-.027	-.045	-.056	-.063	-.066	-.065
.150	+.027	+.023	+.011	-.006	-.027	-.043	-.059	-.070	-.075	-.077	-.077
.165	+.001	-.001	-.013	-.030	-.049	-.066	-.079	-.089	-.093	-.094	-.094
.180	-.021	-.024	-.035	-.051	-.069	-.085	-.095	-.103	-.107	-.107	-.106
.195	-.039	-.041	-.053	-.066	-.084	-.096	-.108	-.114	-.115	-.115	-.115
.210	-.058	-.059	-.070	-.084	-.098	-.112	-.120	-.125	-.125	-.123	-.124
.225	-.067	-.068	-.079	-.092	-.106	-.117	-.124	-.128	-.127	-.125	-.123
.240	-.073	-.074	-.084	-.095	-.108	-.119	-.126	-.127	-.126	-.124	-.122
.255	-.086	-.086	-.097	-.109	-.119	-.128	-.133	-.133	-.131	-.126	-.125
.270	-.098	-.098	-.108	-.118	-.128	-.135	-.138	-.137	-.133	-.128	-.127
.285	-.102	-.101	-.110	-.120	-.129	-.135	-.137	-.134	-.129	-.124	-.122
.300	-.106	-.105	-.115	-.124	-.132	-.136	-.136	-.132	-.125	-.118	-.117
.315	-.108	-.107	-.116	-.123	-.131	-.134	-.132	-.127	-.119	-.112	-.110
.330	-.104	-.103	-.112	-.119	-.125	-.127	-.124	-.117	-.109	-.101	-.099
.360	-.077	-.076	-.084	-.090	-.093	-.093	-.089	-.081	-.071	-.063	-.060
.390	-.053	-.051	-.060	-.065	-.068	-.066	-.060	-.051	-.040	-.032	-.029
.420	-.027	-.026	-.034	-.038	-.042	-.040	-.034	-.026	-.017	-.011	-.008
.450	-.025	-.023	-.032	-.037	-.040	-.037	-.030	-.021	-.012	-.005	-.002
.480	-.020	-.018	-.027	-.031	-.033	-.031	-.023	-.014	-.006	+.000	+.003
.520	-.007	-.005	-.013	-.018	-.020	-.019	-.012	-.004	+.003	+.008	+.011
.550	-.007	-.005	-.014	-.017	-.019	-.016	-.010	-.002	+.003	+.008	+.011
.580	-.007	-.006	-.014	-.017	-.019	-.016	-.009	-.001	+.004	+.008	+.011
.621	-.000	+.000	-.008	-.011	-.013	-.009	-.002	+.003	+.008	+.012	+.015
.640	-.004	-.003	-.011	-.014	-.015	-.011	-.003	+.003	+.007	+.010	+.013
.670	+.001	+.003	-.004	-.007	-.008	-.004	+.002	+.006	+.009	+.013	+.016
.700	+.007	+.009	-.000	-.003	-.004	-.000	+.005	+.008	+.010	+.015	+.019
.730	+.006	+.008	+.000	-.001	-.002	+.001	+.007	+.010	+.011	+.015	+.019
.760	+.004	+.006	+.000	-.001	+.000	+.003	+.008	+.010	+.012	+.015	+.020

Table 1

PRESSURE COEFFICIENT

INCIDENCE= 4

ROLL ANGLE

X/L	0	18	36	54	72	90	108	126	144	162	180
.015	+.363	+.359	+.342	+.319	+.295	+.269	+.250	+.234	+.223	+.218	+.216
.030	+.292	+.285	+.271	+.250	+.227	+.205	+.184	+.169	+.158	+.153	+.150
.045	+.241	+.237	+.223	+.205	+.181	+.160	+.142	+.126	+.116	+.110	+.107
.060	+.201	+.196	+.188	+.171	+.149	+.130	+.112	+.099	+.091	+.086	+.080
.075	+.148	+.146	+.135	+.117	+.097	+.078	+.060	+.048	+.039	+.032	+.031
.090	+.115	+.113	+.105	+.088	+.069	+.051	+.033	+.020	+.012	+.006	+.005
.105	+.083	+.081	+.073	+.057	+.040	+.022	+.007	-.006	-.013	-.019	-.021
.120	+.058	+.056	+.050	+.035	+.018	+.001	-.012	-.024	-.032	-.037	-.039
.135	+.033	+.032	+.025	+.012	-.005	-.021	-.035	-.044	-.052	-.056	-.057
.150	+.012	+.013	+.006	-.006	-.022	-.036	-.050	-.059	-.066	-.068	-.070
.165	-.013	-.011	-.019	-.029	-.044	-.058	-.070	-.079	+.084	-.087	-.088
.180	-.033	-.034	-.039	-.050	-.064	-.077	-.087	-.094	-.099	-.101	-.101
.195	-.051	-.052	-.056	-.066	-.080	-.091	-.100	-.106	-.110	-.110	-.111
.210	-.069	-.069	-.073	-.083	-.095	-.105	-.113	-.118	-.120	-.121	-.121
.225	-.078	-.077	-.081	-.091	-.102	-.111	-.117	-.121	-.123	-.123	-.122
.240	-.084	-.082	-.087	-.095	-.105	-.114	-.119	-.122	-.122	-.122	-.122
.255	-.096	-.095	-.098	-.107	-.115	-.123	-.127	-.129	-.128	-.126	-.126
.270	-.108	-.107	-.110	-.117	-.125	-.130	-.133	-.133	-.131	-.129	-.128
.285	-.109	-.109	-.111	-.118	-.125	-.130	-.131	-.131	-.128	-.126	-.124
.300	-.113	-.112	-.115	-.122	-.127	-.130	-.131	-.130	-.125	-.121	-.119
.315	-.115	-.113	-.116	-.121	-.126	-.128	-.127	-.125	-.120	-.116	-.114
.330	-.110	-.109	-.111	-.116	-.120	-.122	-.120	-.116	-.110	-.105	-.103
.360	-.082	-.081	-.083	-.086	-.089	-.089	-.086	-.080	-.073	-.068	-.065
.390	-.056	-.056	-.058	-.061	-.062	-.061	-.057	-.051	-.042	-.036	-.034
.420	-.031	-.030	-.031	-.034	-.036	-.035	-.031	-.025	-.018	-.014	-.012
.450	-.029	-.028	-.030	-.032	-.033	+.032	-.027	-.021	-.013	-.008	-.006
.480	-.023	-.022	-.024	-.026	-.027	-.025	-.021	-.014	-.007	-.003	-.001
.520	-.011	-.010	-.011	-.012	-.014	-.012	-.008	-.003	+.002	+.006	+.008
.550	-.011	-.010	-.011	-.012	-.014	-.012	-.007	-.001	+.003	+.006	+.008
.580	-.011	-.010	-.011	-.013	-.013	-.011	-.006	+.000	+.003	+.007	+.008
.621	-.004	-.003	-.005	-.007	-.007	-.005	+.000	+.004	+.008	+.011	+.013
.640	-.008	-.008	-.008	-.009	-.010	-.007	-.002	+.003	+.007	+.009	+.011
.670	-.002	-.000	-.002	-.003	-.003	+.000	+.003	+.007	+.009	+.012	+.014
.700	+.002	+.003	+.003	+.002	+.002	+.004	+.008	+.010	+.012	+.014	+.017
.730	+.002	+.003	+.002	+.001	+.002	+.005	+.009	+.011	+.013	+.015	+.017
.760	-.000	+.001	+.002	+.002	+.003	+.006	+.010	+.012	+.014	+.015	+.018

Table 2

PRESSURE COEFFICIENT

INCIDENCE= 3

ROLL ANGLE

X/L	0	18	36	54	72	90	108	126	144	162	180
.015	+.335	+.336	+.328	+.316	+.304	+.287	+.273	+.261	+.251	+.246	+.244
.030	+.264	+.265	+.258	+.250	+.239	+.220	+.205	+.193	+.184	+.178	+.175
.045	+.216	+.217	+.213	+.203	+.189	+.175	+.160	+.148	+.139	+.133	+.132
.060	+.179	+.179	+.177	+.167	+.156	+.142	+.130	+.119	+.110	+.105	+.104
.075	+.125	+.125	+.123	+.116	+.104	+.090	+.077	+.066	+.058	+.052	+.050
.090	+.093	+.094	+.093	+.085	+.074	+.061	+.049	+.037	+.029	+.025	+.022
.105	+.063	+.064	+.063	+.056	+.044	+.032	+.019	+.009	+.002	-.002	-.003
.120	+.039	+.041	+.039	+.034	+.023	+.011	-.000	-.009	-.016	-.021	-.022
.135	+.015	+.017	+.014	+.009	+.000	-.012	-.022	-.031	-.036	-.041	-.042
.150	-.003	-.001	-.003	-.008	-.018	-.028	-.039	-.047	-.052	-.055	-.056
.165	-.027	-.025	-.026	-.032	-.040	-.050	-.060	-.067	-.072	-.075	-.076
.180	-.048	-.046	-.048	-.052	-.060	-.070	-.077	-.083	-.088	-.091	-.092
.195	-.063	-.062	-.063	-.068	-.075	-.084	-.090	-.097	-.099	-.102	-.102
.210	-.081	-.079	-.078	-.083	-.091	-.099	-.104	-.109	-.112	-.113	-.114
.225	-.088	-.086	-.086	-.091	-.098	-.105	-.110	-.114	-.116	-.116	-.117
.240	-.092	-.092	-.092	-.095	-.101	-.107	-.112	-.115	-.116	-.117	-.117
.255	-.103	-.101	-.102	-.106	-.111	-.117	-.120	-.122	-.123	-.122	-.123
.270	-.114	-.112	-.112	-.115	-.119	-.124	-.127	-.128	-.128	-.127	-.127
.285	-.114	-.114	-.114	-.117	-.120	-.124	-.127	-.126	-.125	-.124	-.124
.300	-.116	-.115	-.117	-.118	-.123	-.125	-.127	-.125	-.124	-.122	-.121
.315	-.116	-.115	-.115	-.118	-.121	-.122	-.123	-.122	-.119	-.117	-.116
.330	-.111	-.110	-.111	-.113	-.114	-.116	-.115	-.114	-.111	-.108	-.107
.360	-.081	-.081	-.081	-.082	-.083	-.084	-.082	-.078	-.075	-.072	-.070
.390	-.054	-.054	-.055	-.056	-.056	-.056	-.054	-.050	-.045	-.042	-.040
.420	-.030	-.029	-.030	-.030	-.031	-.030	-.028	-.025	-.021	-.017	-.017
.450	-.027	-.025	-.026	-.027	-.027	-.027	-.024	-.020	-.016	-.012	-.011
.480	-.021	-.020	-.021	-.021	-.021	-.021	-.018	-.014	-.011	-.007	-.006
.520	-.009	-.008	-.008	-.008	-.009	-.008	-.006	-.003	-.000	+.003	+.004
.550	-.009	-.008	-.008	-.008	-.008	-.007	-.006	-.002	+.000	+.004	+.004
.580	-.010	-.008	-.008	-.008	-.008	-.007	-.004	-.001	+.001	+.004	+.005
.621	-.002	-.001	-.002	-.002	-.002	-.001	+.000	+.003	+.006	+.009	+.008
.640	-.005	-.005	-.005	-.005	-.004	-.003	-.000	+.002	+.006	+.008	+.007
.670	-.000	+.000	+.000	+.000	+.001	+.001	+.004	+.007	+.010	+.011	+.010
.700	+.004	+.005	+.005	+.006	+.005	+.007	+.009	+.011	+.012	+.014	+.014
.730	+.003	+.004	+.005	+.005	+.006	+.007	+.009	+.012	+.013	+.015	+.015
.760	+.000	+.002	+.004	+.005	+.006	+.008	+.011	+.013	+.015	+.017	+.016

Table 3

PRESSURE COEFFICIENT

INCIDENCE= 2

ROLL ANGLE

X/L	0	18	36	54	72	90	108	126	144	162	180
.015	+.312	+.313	+.313	+.311	+.306	+.299	+.291	+.283	+.274	+.269	+.263
.030	+.240	+.242	+.245	+.243	+.239	+.233	+.223	+.215	+.207	+.200	+.195
.045	+.194	+.196	+.198	+.196	+.194	+.186	+.178	+.167	+.160	+.154	+.150
.060	+.159	+.160	+.163	+.163	+.158	+.152	+.144	+.135	+.127	+.124	+.120
.075	+.105	+.108	+.110	+.108	+.106	+.099	+.091	+.081	+.075	+.070	+.068
.090	+.074	+.078	+.079	+.078	+.076	+.070	+.061	+.052	+.046	+.040	+.039
.105	+.045	+.049	+.049	+.048	+.045	+.039	+.031	+.023	+.017	+.013	+.011
.120	+.022	+.026	+.027	+.026	+.023	+.017	+.010	+.002	-.003	-.008	-.009
.135	+.000	+.004	+.004	+.003	+.000	-.004	-.011	-.019	-.025	-.028	-.030
.150	-.016	-.013	-.013	-.013	-.017	-.022	-.029	-.036	-.040	-.045	-.045
.165	-.039	-.037	-.036	-.037	-.040	-.046	-.051	-.057	-.062	-.065	-.065
.180	-.058	-.055	-.057	-.057	-.059	-.064	-.069	-.075	-.079	-.081	-.083
.195	-.073	-.070	-.072	-.072	-.075	-.079	-.084	-.089	-.092	-.094	-.095
.210	-.087	-.086	-.087	-.088	-.090	-.094	-.098	-.102	-.105	-.107	-.107
.225	-.094	-.092	-.093	-.094	-.096	-.100	-.104	-.107	-.110	-.110	-.111
.240	-.098	-.096	-.097	-.098	-.100	-.104	-.106	-.110	-.111	-.112	-.113
.255	-.107	-.105	-.108	-.108	-.110	-.113	-.116	-.118	-.119	-.120	-.119
.270	-.116	-.114	-.116	-.117	-.119	-.122	-.123	-.125	-.125	-.125	-.125
.285	-.115	-.114	-.117	-.118	-.119	-.120	-.122	-.124	-.124	-.123	-.123
.300	-.117	-.115	-.118	-.119	-.120	-.121	-.123	-.123	-.122	-.122	-.121
.315	-.116	-.115	-.117	-.118	-.119	-.119	-.121	-.120	-.119	-.118	-.118
.330	-.110	-.107	-.112	-.112	-.112	-.113	-.113	-.113	-.111	-.110	-.109
.360	-.078	-.077	-.081	-.082	-.081	-.081	-.080	-.080	-.077	-.075	-.074
.390	-.051	-.050	-.053	-.054	-.053	-.053	-.052	-.051	-.048	-.046	-.044
.420	-.026	-.025	-.029	-.029	-.028	-.028	-.027	-.026	-.024	-.022	-.020
.450	-.022	-.021	-.025	-.025	-.024	-.024	-.023	-.022	-.019	-.017	-.016
.480	-.017	-.016	-.020	-.019	-.019	-.018	-.017	-.016	-.013	-.011	-.010
.520	-.004	-.004	-.008	-.007	-.007	-.007	-.006	-.004	-.002	-.000	+.000
.550	-.004	-.004	-.007	-.007	-.006	-.006	-.005	-.004	-.001	+.000	+.001
.580	-.004	-.003	-.007	-.007	-.006	-.006	-.004	-.003	-.001	+.000	+.002
.621	+.001	+.002	-.001	-.001	-.000	+.000	+.001	+.002	+.004	+.005	+.007
.640	-.000	-.000	-.003	-.003	-.002	-.002	-.000	+.000	+.003	+.004	+.005
.670	+.005	+.004	+.001	+.001	+.002	+.003	+.004	+.006	+.007	+.009	+.010
.700	+.008	+.009	+.005	+.006	+.007	+.008	+.008	+.009	+.011	+.012	+.013
.730	+.008	+.008	+.005	+.006	+.007	+.008	+.009	+.011	+.012	+.013	+.015
.760	+.005	+.006	+.003	+.005	+.007	+.009	+.010	+.012	+.014	+.016	+.016

Table 4

PRESSURE COEFFICIENT

INCIDENCE= 0

ROLL ANGLE

X/L	0	18	36	54	72	90	108	126	144	162	180
.015	+.266	+.272	+.278	+.286	+.293	+.301	+.309	+.315	+.316	+.314	+.311
.030	+.202	+.206	+.210	+.217	+.227	+.234	+.239	+.243	+.245	+.244	+.242
.045	+.155	+.162	+.167	+.174	+.179	+.187	+.192	+.196	+.198	+.197	+.193
.060	+.127	+.131	+.135	+.141	+.146	+.152	+.158	+.163	+.162	+.160	+.156
.075	+.075	+.078	+.084	+.089	+.093	+.099	+.104	+.107	+.109	+.106	+.104
.090	+.046	+.050	+.056	+.059	+.065	+.069	+.074	+.076	+.078	+.076	+.073
.105	+.019	+.023	+.028	+.031	+.035	+.039	+.044	+.047	+.047	+.045	+.043
.120	-.001	+.002	+.007	+.010	+.014	+.017	+.021	+.024	+.025	+.023	+.021
.135	-.022	-.019	-.014	-.011	-.008	-.005	-.001	+.000	+.000	+.000	-.003
.150	-.038	-.035	-.029	-.028	-.024	-.022	-.020	-.016	-.016	-.018	-.019
.165	-.058	-.055	-.051	-.050	-.047	-.045	-.043	-.040	-.038	-.041	-.043
.180	-.076	-.073	-.069	-.069	-.066	-.065	-.062	-.060	-.059	-.061	-.063
.195	-.089	-.086	-.082	-.083	-.081	-.079	-.076	-.075	-.075	-.076	-.077
.210	-.102	-.100	-.096	-.097	-.095	-.095	-.092	-.090	-.089	-.091	-.092
.225	-.106	-.104	-.101	-.101	-.100	-.099	-.098	-.096	-.096	-.096	-.098
.240	-.108	-.106	-.104	-.105	-.104	-.103	-.101	-.100	-.100	-.101	-.102
.255	-.116	-.114	-.112	-.113	-.113	-.112	-.111	-.110	-.109	-.110	-.111
.270	-.123	-.121	-.119	-.122	-.121	-.121	-.120	-.118	-.118	-.118	-.118
.285	-.122	-.120	-.118	-.122	-.121	-.120	-.119	-.119	-.119	-.118	-.119
.300	-.120	-.118	-.117	-.121	-.120	-.120	-.119	-.119	-.119	-.119	-.119
.315	-.118	-.116	-.115	-.120	-.119	-.119	-.118	-.118	-.118	-.117	-.118
.330	-.110	-.109	-.108	-.112	-.112	-.113	-.112	-.112	-.111	-.110	-.111
.360	-.076	-.075	-.075	-.079	-.080	-.081	-.081	-.080	-.079	-.079	-.079
.390	-.046	-.046	-.046	-.051	-.051	-.053	-.052	-.052	-.052	-.052	-.052
.420	-.023	-.021	-.022	-.026	-.027	-.028	-.027	-.027	-.026	-.026	-.026
.450	-.017	-.016	-.017	-.022	-.023	-.023	-.023	-.023	-.023	-.023	-.022
.480	-.012	-.011	-.011	-.016	-.017	-.018	-.018	-.018	-.017	-.017	-.017
.520	-.001	+.000	+.000	-.005	-.006	-.006	-.006	-.006	-.005	-.005	-.005
.550	+.000	+.001	+.000	-.004	-.005	-.005	-.005	-.005	-.004	-.005	-.004
.580	+.000	+.002	+.001	-.004	-.004	-.005	-.005	-.005	-.004	-.004	-.004
.621	+.006	+.008	+.007	+.002	+.001	+.007	+.001	+.000	+.002	+.001	+.002
.640	+.004	+.006	+.005	+.000	-.001	-.001	-.001	-.001	+.000	+.000	+.000
.670	+.008	+.010	+.010	+.005	+.004	+.003	+.004	+.004	+.005	+.004	+.005
.700	+.009	+.014	+.012	+.008	+.007	+.007	+.007	+.008	+.008	+.009	+.009
.730	+.010	+.013	+.013	+.008	+.007	+.008	+.009	+.010	+.011	+.012	+.012
.760	+.006	+.010	+.009	+.006	+.007	+.008	+.011	+.013	+.015	+.016	+.017

Table 5

PRESSURE COEFFICIENT

INCIDENCE=-2

ROLL ANGLE

X/L	0	18	36	54	72	90	108	126	144	162	180
.015	+.232	+.236	+.244	+.256	+.272	+.290	+.309	+.328	+.341	+.347	+.346
.030	+.168	+.172	+.179	+.191	+.204	+.222	+.240	+.256	+.272	+.278	+.277
.045	+.126	+.129	+.137	+.147	+.160	+.178	+.195	+.211	+.224	+.229	+.228
.060	+.101	+.105	+.110	+.118	+.129	+.145	+.161	+.174	+.185	+.192	+.190
.075	+.048	+.050	+.056	+.064	+.076	+.090	+.105	+.119	+.130	+.137	+.136
.090	+.021	+.024	+.029	+.037	+.047	+.060	+.075	+.087	+.099	+.105	+.104
.105	-.004	-.001	+.003	+.010	+.019	+.032	+.045	+.056	+.067	+.074	+.073
.120	-.022	-.020	-.015	-.010	-.000	+.009	+.021	+.034	+.044	+.050	+.050
.135	-.042	-.039	-.035	-.030	-.022	-.012	-.000	+.009	+.019	+.025	+.024
.150	-.056	-.054	-.049	-.045	-.037	-.028	-.018	-.008	+.000	+.006	+.006
.165	-.076	-.073	-.069	-.066	-.059	-.051	-.041	-.032	-.024	-.018	-.019
.180	-.091	-.088	-.087	-.082	-.077	-.069	-.061	-.052	-.045	-.040	-.040
.195	-.102	-.100	-.098	-.095	-.091	-.085	-.077	-.069	-.061	-.056	-.057
.210	-.114	-.112	-.111	-.109	-.104	-.099	-.093	-.085	-.078	-.073	-.074
.225	-.116	-.115	-.113	-.112	-.109	-.104	-.098	-.092	-.086	-.081	-.082
.240	-.117	-.116	-.115	-.115	-.111	-.108	-.102	-.096	-.091	-.087	-.087
.255	-.123	-.122	-.123	-.123	-.120	-.117	-.113	-.107	-.102	-.098	-.099
.270	-.128	-.128	-.128	-.129	-.127	-.125	-.121	-.117	-.112	-.109	-.110
.285	-.124	-.126	-.126	-.126	-.126	-.124	-.122	-.118	-.114	-.111	-.111
.300	-.121	-.122	-.124	-.126	-.124	-.124	-.121	-.118	-.116	-.114	-.114
.315	-.117	-.119	-.121	-.123	-.124	-.123	-.122	-.119	-.117	-.114	-.114
.330	-.108	-.110	-.112	-.115	-.116	-.116	-.116	-.114	-.112	-.110	-.110
.360	-.071	-.074	-.077	-.081	-.083	-.084	-.085	-.083	-.083	-.080	-.081
.390	-.041	-.044	-.047	-.051	-.054	-.056	-.057	-.057	-.055	-.054	-.055
.420	-.018	-.019	-.023	-.027	-.030	-.032	-.033	-.032	-.030	-.028	-.029
.450	-.012	-.014	-.018	-.022	-.025	-.027	-.028	-.028	-.028	-.026	-.026
.480	-.006	-.008	-.012	-.016	-.019	-.022	-.023	-.023	-.022	-.021	-.021
.520	+.003	+.002	-.001	-.004	-.008	-.009	-.011	-.010	-.009	-.008	-.008
.550	+.004	+.002	-.000	-.003	-.007	-.009	-.010	-.010	-.009	-.008	-.008
.580	+.004	+.003	-.000	-.003	-.006	-.008	-.010	-.010	-.009	-.007	-.008
.621	+.010	+.008	+.006	+.002	-.000	-.002	-.003	-.003	-.002	-.001	-.001
.640	+.008	+.007	+.004	+.001	-.002	-.004	-.006	-.006	-.005	-.004	-.004
.670	+.011	+.010	+.008	+.005	+.002	+.000	-.001	-.000	+.000	+.001	+.001
.700	+.012	+.011	+.010	+.007	+.005	+.004	+.003	+.004	+.005	+.007	+.005
.730	+.012	+.011	+.010	+.008	+.006	+.005	+.004	+.005	+.008	+.009	+.009
.760	+.007	+.007	+.007	+.006	+.005	+.005	+.006	+.008	+.011	+.014	+.014

Table 6